# DESIGN AND PERFORMANCE ANALYSIS OF ARTIFICIAL INTELLIGENCE BASED MAXIMUM POWER POINT TRACKING ALGORITHMS FOR PV ARRAY UNDER PARTIAL SHADING CONDITIONS

A
THESIS

SUBMITTED IN PARTIAL FULFILMENT OF THE REQUIREMENT
FOR THE AWARD OF THE DEGREE OF

**MASTER OF TECHNOLOGY**

**In**

**POWER SYSTEMS**

**by**

Shagun Chaudhary
(2K19/PSY/17)

**UNDER THE GUIDANCE OF**

**Dr. Alka Singh**
**Professor**
**Department of Electrical Engineering**


**DELHI TECHNOLOGICAL UNIVERSITY, DELHI**
**July 2021**

# DECLARATION

This is to certify that the thesis entitled "**Design and Performance Analysis of Artificial Intelligence based Maximum Power Point Tracking Algorithms for PV Array under Partial Shading Conditions**" which is submitted by me in the partial fulfillment of the requirement for the award of degree Master of Technology in Power Systems to Delhi Technological University, Delhi comprises only my own work and due acknowledgement has been made in the text to all other material used.

**Date:** 28 July 2021

**Shagun Chaudhary**

(2K19/PSY/17)

# CERTIFICATE

This is to certify that thesis entitled "**Design and Performance Analysis of Artificial Intelligence based Maximum Power Point Tracking Algorithms for PV Array under Partial Shading Conditions**" which is submitted by **Shagun Chaudhary** (2K19/PSY/17) in partial fulfillment of the requirement for the award of degree Master of Technology in Power Systems to Delhi Technological University, Delhi is a record of the candidate's own work carried out by her under my supervision. The matter embodied in this report is original and has not been submitted for the award of any other degree.

**Date:**

**Dr. Alka Singh**
Professor
Department of Electrical Engineering
Delhi Technological University
Delhi

# Abstract

Sustainability is the ability of a resource to be viable between generations and not get exhausted or affect the nature directly or indirectly. The rapidly increasing demand and the inability of the conventionally utilized fossil fuels does not add to the sustainability of the environment. It not only pollutes the environment via its fumes but also leaves a large carbon footprint. Renewable energy sources are the sources which do not exhaust over time. Solar energy is a widely used source of energy due to the abundant availability of sunlight all over the world.

The main objective of any generation activity deals with the maximization of benefits and revenue. This revenue depends upon the generation by the plant, which in turn depends on the plant performance. Thus, a maximization of the plant performance i.e., the output power is desirable. This maximization of power can be obtained from a PV array by operating it at its maximum power point i.e., the MPP of the designed array.

Various MPP techniques are employed for this purpose and they vary from each other on the basis of their inherent structure, the logic behind the algorithm, the convergence as well as computation time. Uniformity of irradiance is a rare phenomenon in the field of solar power generation. However, testing of the PV arrays is done at STC i.e., 1000 $W/m^2$ irradiance at a temperature of 25˚C or 298 K. Conventionally available techniques have been used over years. However, the inherent oscillations in their response and the relatively poor tracking speeds have acted as a motivation for the development of Artificial Intelligence (AI) based techniques.

The AI based techniques employ the basic input required by the conventional techniques along with an additional change in error of these inputs. This gives these techniques an effective direction for locating and approaching the MPP at a faster speed within least possible time. The three main AI based controllers are Fuzzy Logic Controller (FLC), Artificial Neural Network (ANN) and Adaptive Neuro-Fuzzy Inference Systems (ANFIS). Rigorous comparative studies are performed on the controllers and a continuous effort is put in to further boost their performance as compared to their conventionally available counterparts by incorporating one modification or the other. A simplified and optimized FLC (SOFLC) is proposed, designed and tested to approximate the performance of a 49-rule base FLC which acts as a trade-off between complexity and accuracy by merely 4 rules and a compensating polynomial.

# Acknowledgement

I express my sincere gratitude to **Dr. Alka Singh**, Professor, Department of Electrical Engineering, Delhi Technological University, Delhi, for her valuable guidance, continuous encouragement and supervision throughout the course of present work. I am deeply indebted to her for the patience and unlimited support offered by her. Her insightful and gentle guidance gave me a clearer perspective on the scientific process that is the real essence of research.

I would like to place on record my deep sense of gratitude to **Prof. Uma Nangia**, Head of Department of Electrical Engineering, Delhi Technological University, Delhi, for her generous guidance, help and useful suggestions.

I also wish to extend my thanks to my seniors Mr. Hemant Saxena, Mr. Allu Bhargava and colleagues for their insightful comments and constructive suggestions to improve the quality of this research work.

I am also thankful to my parents and family members for their constant support and encouragement. They have always been a motivating force for me.

Most importantly, I am grateful to my teachers and parents, for everything they have done to shape my life. To them, I dedicate this thesis.

**Shagun Chaudhary**

(2K19/PSY/17)

# CONTENTS

# LIST OF FIGURES

# LIST OF TABLES

# Chapter 1

# Introduction

## 1.1 OVERVIEW

In a world where the demand for electricity reaches a new high on a regular basis, it is worth noting that the power generation sector itself contributed to 75% of the total carbon footprint in the world [1]. According to the Global Energy & $CO_2$ Status Report 2019, the global $CO_2$ emissions related to energy rose by 1.7% in 2018 and amounted to two-thirds of the global $CO_2$ emissions [2]. A stacked line chart representing the global energy-related carbon dioxide emissions has been illustrated in Fig. 1.1. The three main contributing factors to the carbon dioxide emissions globally are coal-fired power generation, other coal use and other fossil fuels. Thus, it is essential to comply with sustainable measures for energy production.

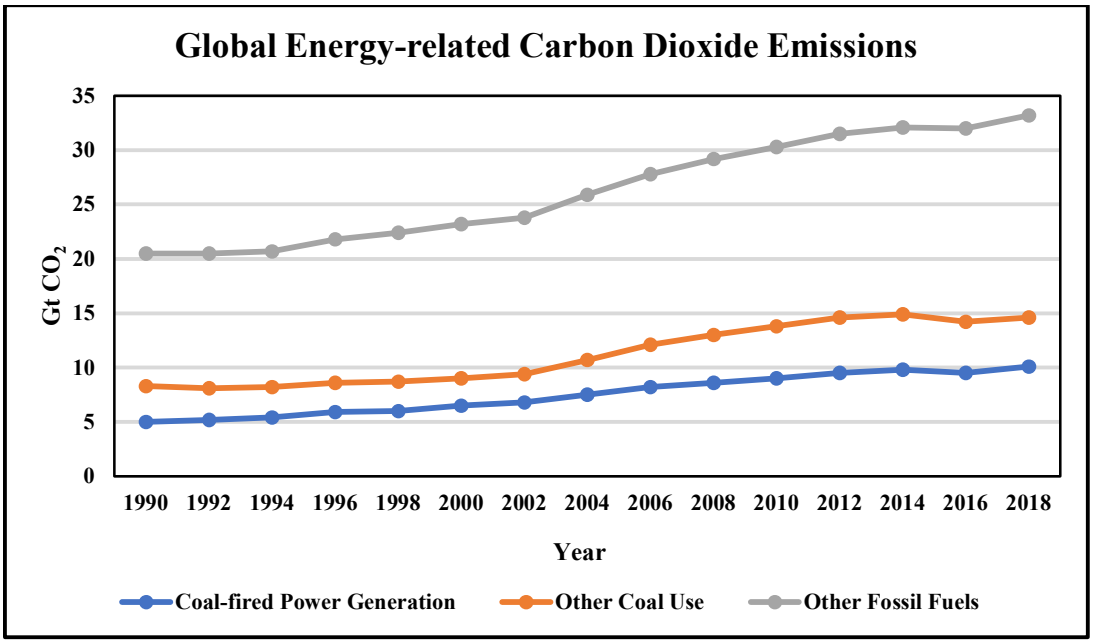


**Fig. 1.1 Global Energy-related Carbon Dioxide Emissions for 2021**

Various sustainable development goals have been put into action in developed as well as developing countries for reducing the carbon emissions from energy generation. Renewable energy resources have been a suitable choice for the fulfillment of these sustainable goals. Not only do they help meet the energy demands, but they also reduce the effects of climate change and reduce the dependence on fossil fuel-based energy consumption [3]. Renewable energy resources have an added advantage of getting replenished over time which has not possible in the case of fossil fuels. These sources of energy have almost negligible carbon footprint and reduce air pollution unlike conventional sources like coal which caused an increase in the concentration of Sulphur Dioxide ($SO_2$) and Nitrogen Oxide ($NO_x$).

Based on the data from the Central Electricity Authority (CEA) and Ministry of New and Renewable Energy (MNRE), the installed capacity of India stood at 382.73 GW as on 28$^{th}$February 2021 [4]. Of this installed capacity, thermal based fuels, which comprised of coal, lignite, gas and diesel, constituted a large portion of 61.5% of the net capacity while renewable energy resources (excluding hydroelectric power) had a significant share of 24.5% of the total installed capacity. Hydro-electric power had a share of 12.2% while nuclear energy contributed 1.8% to the total capacity. This contribution from the various sources of energy has been depicted in Fig. 1.2.

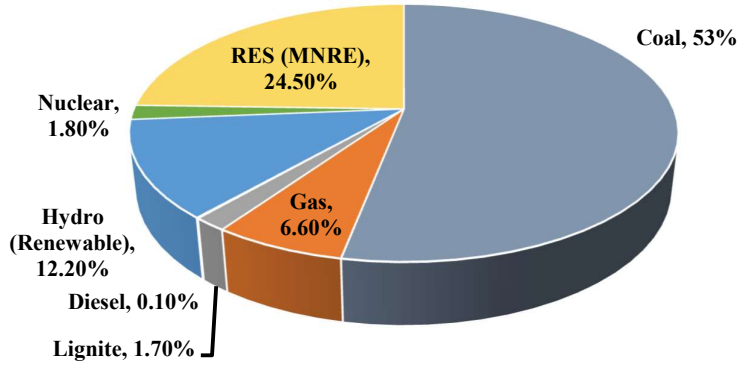


**Fig. 1.2 Share of Various Sources in Net Installed Capacity based on CEA Report, Feb 2021.**

Various forms of renewable energy include, but are not limited to, solar energy, wind energy, biomass energy, tidal energy, geothermal energy, and small hydro power. A classification of the renewable energy sources has been shown in Fig. 1.3. Renewable sources of energy are distributed over a large area as compared to conventional sources like coal and diesel which are concentrated at certain locations. These non-conventional sources of energy are eco-friendly and sustainable. This will help the developing nations to bring an overall increase in their growth rates of energy generation and not be completely dependent over imported fossil fuels.

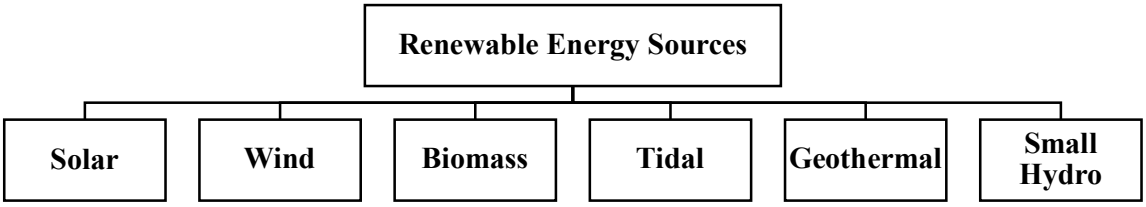


**Fig. 1.3 Types of Renewable Energy Sources**

In the Indian scenario, solar energy is preferred over other forms of renewable energy. Abundant availability of solar energy in India makes it the most suitable alternative among the available renewable sources of power generation. However, high wind velocities also give India, a huge potential for wind energy. Due to a large number of rivers and tributaries, small hydro power generation is also a possible source. There is also a significant amount of generation of energy via biomass in India.

## 1.2 SOLAR ENERGY

Solar energy is the one of the most preferable energy sources across the globe. The abundant availability along with the sustainable form of power generation makes it a perfect choice for domestic as well as industrial applications. The incentives provided by the governments of countries all around the world have also provided a boost to the solar based power generation as it has made solar more affordable for domestic applications.

Solar energy is the energy extracted from a solar cell which has been under constant exposure of the sun. Solar energy can either be generated using the direct as well as indirect methods. Concentrated solar power is an indirect type of power generation technique and is generally used for high power applications. Concentrated solar energy can be generated by two technologies, which are solar thermal and solar photovoltaic (PV) [5].

In solar thermal technology, large sized mirrors and lenses are employed along with efficient tracking system in order to track the position of the sun and with the help of the mirrors and lenses to concentrate the sun rays in a small area to produce heat. This heat could further be used for various applications like water heating and space heating. Usually, parabolic concentrators are used for this purpose as they can generate higher temperatures of the order of 200-300˚C due to their better focusing capabilities.

In concentrated solar photovoltaic technology, solar power is concentrated upon PV panels for the purpose of electricity generation. A hybrid concentrated solar energy system would include the use of both the concentrated solar power-based techniques to generate electricity along with heat.

Solar photovoltaic technology involves the use of PV cells to directly convert light energy in the form of sun rays into electrical energy. This technology has emerged as the best alternative for remote locations where power from conventional sources of energy or grid is unavailable. The grid integration of these PV panels gives a boost not only to the utility but also the consumers in general. The consumer is no longer just a consumer for the grid but also a potential supplier of energy during peak hours.

## 1.3 PV CELL

A PV cell is the smallest building block of a PV module or a PV array. It is an electrical device responsible for conversion of incident light into electrical energy [6].

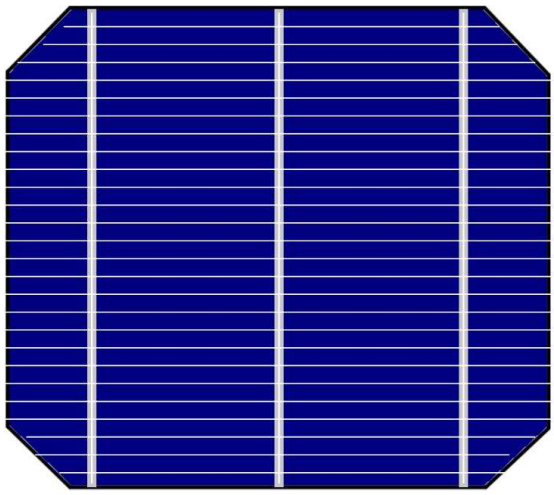

**Fig. 1.4 PV Cell**

The solar cells are considered photovoltaic i.e., producing energy by converting the energy of the incident light irrespective of the source of light. The operation of a PV cell includes three salient features [7, 8]:

- Absorption of light which generates electron-hole pair combinations.
- Separation of charge carriers of opposite polarities.
- Collection of the oppositely charged carriers through an external circuit.

## 1.4 MATHEMATICAL MODEL OF A PV CELL

The datasheets usually offer limited information and the results obtained from the different units could vary. Thus, an accurate mathematical model of a PV cell is essential for simulating and conducting studies on a PV module. A PV cell can be mathematically modeled broadly in two ways: single diode model and double diode model [9]. This classification is based on the number of diodes used in the equivalent circuit of the PV cell and is shown in Fig. 1.5.

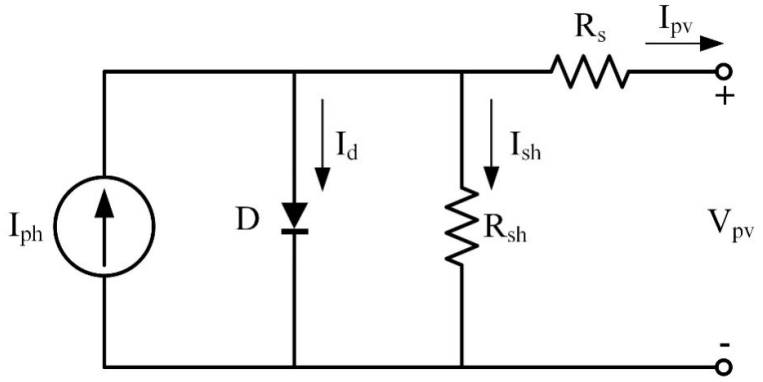


**(a)**

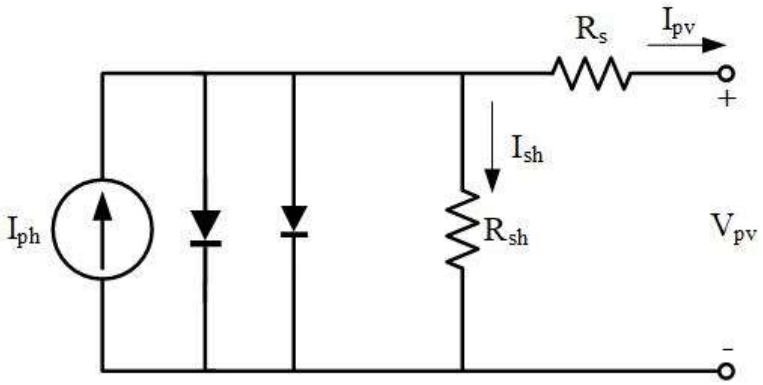


**(b)**

**Fig. 1.5 (a) Single-diode equivalent model and (b) Double-diode equivalent model of a PV cell**

The single diode model of a PV cell is used in this work due to its reduced complexity. The ideal equivalent model of a PV cell has been shown in Fig. 1.6 (a). It includes a current source connected in parallel with a diode. Even though, the ideal equivalent model is the simplest model of a PV cell, it does not take into account the practical conditions. In this case, a practical model of a PV cell is used. The practical equivalent model of a PV cell has been shown in Fig. 1.6 (b).

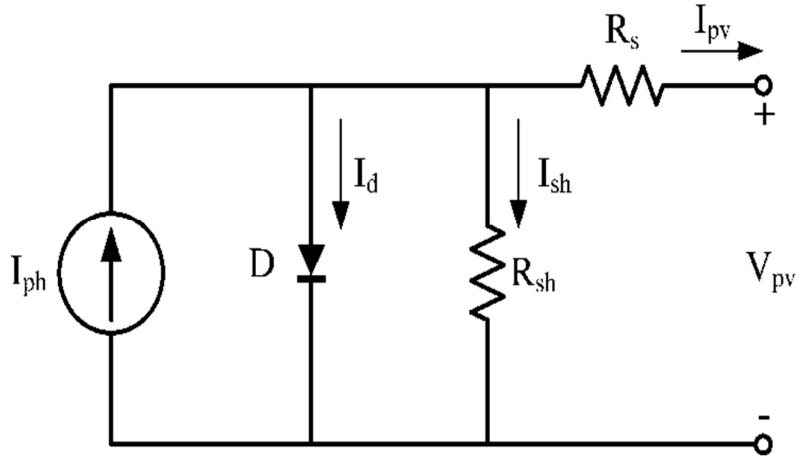


**Fig. 1.6 Practical Equivalent Model of a PV cell**

The practical equivalent model consists of a combination of shunt and series resistance connected to the ideal equivalent model of the PV cell [10-14]. Thus, the current produced by the PV cell, $I_{pv}$ (A), can be computed as the difference of the sum of diode current, $I_d$ (A), and the current through the resistor connected in parallel with the cell, $I_p$ (A), from the photo-current generated by the PV cell, $I_{ph}$, due to the incident irradiation as shown in eqn. (1.1).

$$I_{pv} = I_{ph} - I_d - I_p \tag{1.1}$$

The photo-current generated by the PV cell depends upon the short-circuit current of the PV cell, $I_{sc}$ (A), operating as well as reference temperature (K), $T_{op}$ and $T_{ref}$ respectively, operating as well as reference irradiance (W/m$^2$), $G_{op}$ and $G_{ref}$ respectively. A slight variation in the short circuit current is observed with a change in the temperature. This change is taken into account in the form of short-circuit temperature coefficient, $K_i$ (%/˚C). Generally, the reference values of $G_{ref}$ and $T_{ref}$ are taken as the values at STC i.e., an irradiance of 1000 W/m$^2$ and a temperature of 25˚C. Thus, the expression for the photo-current can be formulated as (1.2).

$$I_{ph} = I_{sc}\left(\frac{G}{G_{ref}}\right)\left[1 + K_i(T_{op} - T_{ref})\right] \tag{1.2}$$

Meanwhile, the diode current is dependent upon factors such as reverse saturation current, $I_o$ (A), diode's ideality factor, A, and the thermal voltage of the diode, $V_T$ (V). The diode current can thus be computed by (1.3).

$$I_d = I_o\left(e^{\frac{(V_{pv}+IR_S)}{AV_T}} - 1\right) \tag{1.3}$$

The expression for thermal voltage may be written as (1.4) in the terms of operating temperature, $T_{op}$(K), Boltzmann's constant ($m^2$ kg $s^{-2}$ $K^{-1}$) and the charge on an electron (C).

$$V_T = \frac{kT_{op}}{q} \tag{1.4}$$

The current passing through the parallel resistance is calculated using (1.5).

$$I_p = \frac{V_{pv}+I_{pv}R_S}{R_p} \tag{1.5}$$

Thus, the expression for output current of the PV cell ($I_{pv}$) can be evaluated as (1.6).

$$I_{pv} = I_{sc}\left(\frac{G}{G_{ref}}\right)\left[1 + K_i(T_{op} - T_{ref})\right] - I_o\left(e^{\frac{(V_{pv}+IR_S)}{AV_T}} - 1\right) - \frac{V_{pv}+I_{pv}R_S}{R_p} \tag{1.6}$$

where the reverse saturation current of the diode, $I_o$ (A), can further be computed in the terms of reverse current, $I_{rs}$ (A) and energy band gap, $E_g$ in eV as (1.7).

$$I_o = I_{rs}\, exp\left[\left(\frac{1}{T_{op}} - \frac{1}{T_{ref}}\right)\frac{E_g q}{Ak}\right]\left(\frac{T_{op}}{T_{ref}}\right)^3 \tag{1.7}$$

## 1.5 PV ARRAY

A PV cell is the basic entity of a PV based system. However, the power output for a PV cell is very small. In order to increase this output for the cells to be used in various applications, the cells are connected in series as well as parallel configurations or a combination of the two. This enhances the current and voltage ratings of the overall structure and thus increases the output power.

A PV module is combination of PV cells connected in series, parallel or series-parallel configuration. The number of cells required for a module can be calculated according to the required ratings for the module. Number of cells in series can be computed using (1.8).

$$No.of\ cells\ in\ series = \frac{Voltage\ rating\ of\ the\ module}{V_{oc}\ of\ a\ PV\ cell} \tag{1.8}$$

In a similar manner, the number of cells in parallel can be calculated as (1.9).

$$No.of\ cells\ in\ parallel = \frac{Current\ rating\ of\ the\ module}{I_{sc}\ of\ a\ PV\ cell} \tag{1.9}$$

Similarly, a PV module is the basic entity for a PV array. An electrically connected combination of modules adds up to a PV array. The calculations of number of modules to be connected in series and parallel can be done using (1.10) and (1.11).

$$No.of\ modules\ in\ series = \frac{Voltage\ rating\ of\ the\ array}{V_{oc}\ of\ a\ PV\ module} \tag{1.10}$$

$$No.of\ modules\ in\ parallel = \frac{Current\ rating\ of\ the\ module}{I_{sc}\ of\ a\ PV\ module} \tag{1.11}$$

For a PV array with $N_s$ modules connected in series and $N_p$ modules connected in parallel, the output current of the array can be given by (1.12).

$$I_{pv} = N_p I_{ph} - N_p I_o \left( e^{\frac{V_{pv} + I R_s \left(\frac{N_s}{N_p}\right)}{A V_T}} - 1 \right) - \frac{V_{pv} + I_{pv} R_s \left(\frac{N_s}{N_p}\right)}{R_p \left(\frac{N_s}{N_p}\right)} \tag{1.12}$$

## 1.6 TYPES OF PV SYSTEMS

PV systems can be broadly categorized into three main categories:

- Stand-alone System
- Grid-tied System
- Hybrid System

**Stand-Alone PV System:** A stand-alone PV system employs only the use of solar energy generated by the PV arrays. It acts as the best alternative for remote locations where extension of power transmission lines would cost even more. This also brings up a self-sufficient and a self-sustaining system of power generation. In order to ensure a 24x7 availability of electricity, a battery storage is required. This battery-based storage gets charged during the day when abundant sunlight is available and during the night, the battery acts as a source for the domestic load. An inverter is used for the conversion of DC output from the PV array to supply an AC output.

**Grid-Tied System:** A grid-tied system not only utilizes the energy from the sun but also avails the benefits of supply from the grid. Thus, the utility grid acts as a virtual battery. When there is an abundant generation by the PV panels, the power is fed into the grid and thus the consumer of the utility, now acts as the supplier to the utility. However, during the time the generation from the PV dips, the domestic load is fed by the grid. Smart meters are installed at the consumer premises for recording the net export and import from the grid.

**Hybrid System:** A hybrid PV system is the combination of the concepts of stand-alone and grid-tied systems. They incorporate an additional battery storage component apart from the grid-tied system. In other words, it can be described as a stand-alone PV system with utility as a backup source for energy.

## 1.7 I-V & P-V CHARACTERISTICS OF A PV CELL

A PV cell and its derivables i.e., modules and array have a non-linear I-V and P-V characteristics as can be observed in Fig 1.7. The power delivered by the cell can hence be derived by the product of the instantaneous voltage and current values. These instantaneous values of power can then be plotted against voltage on the x-axis to obtain the P-V characteristics of the PV cell.

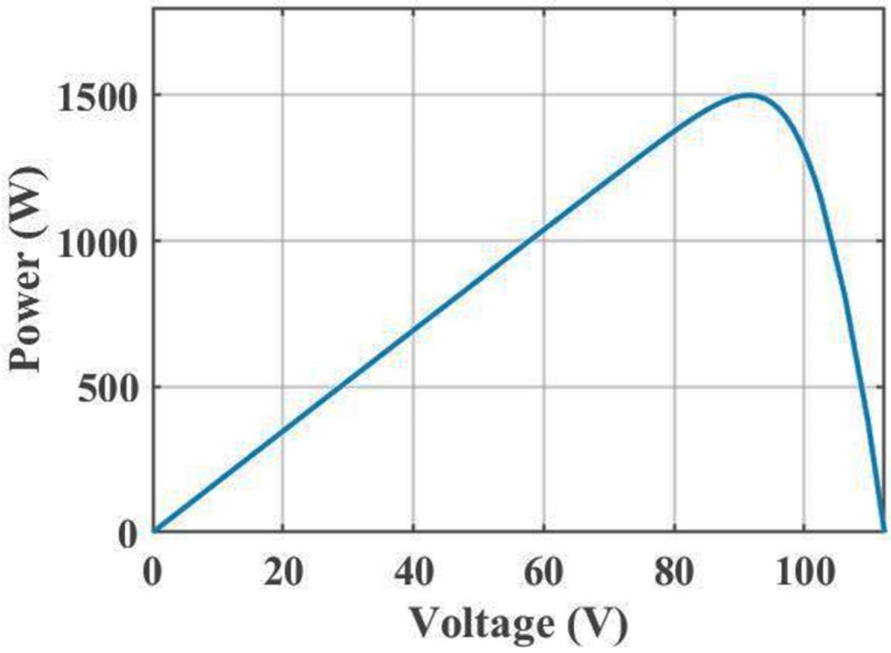


**(a)**

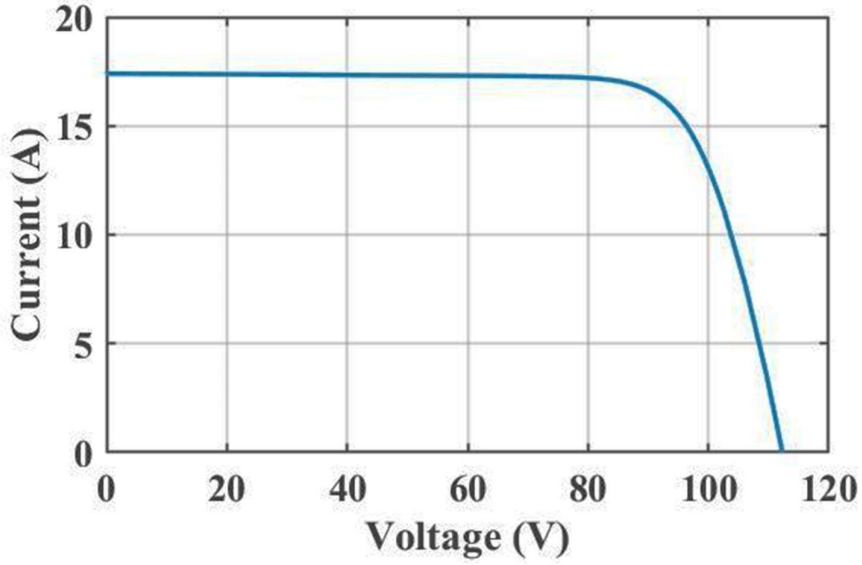


**(b)**

**Fig. 1.7 I-V and P-V Characteristics of a combination of PV cells**

Under open-circuit condition, no load is connected to the cell and thus the current through it will be minimum (zero under ideal case) and the voltage across it would be maximum. This maximum voltage is termed as the open-circuit voltage of a PV cell. It can be denoted as $V_{oc}$. Similarly, under short-circuit condition, the voltage across the cell takes a minimum value (zero under ideal case) and the current through it would be maximum. This maximum current is known as the short-circuit current of a PV cell, which is represented as $I_{sc}$.

Thus, the PV cell operates in a region enclosed by current ranging from 0 A to $I_{sc}$ A and voltage ranging from 0 V to $V_{oc}$ V. However, no power is obtained at either of these extremes. But there would be a point between these extreme points where the power obtained from the PV cell will be maximum i.e., the maximum power point (MPP). This maximum point is obtained at a combination of current and voltage values such that the current at the MPP is approximately 0.85 to 0.95 times the short-circuit current $I_{sc}$ and the voltage at the MPP is around 0.8 to 0.9 times the open-circuit voltage $V_{oc}$.

## 1.8 I-V& P-V CHARACTERISTICS OF A PV ARRAY

A PV array contains modules connected in series or parallel. This serial and parallel connection modifies the overall open-circuit and short-circuit limits. In the case of series connection, the voltage across the array terminals increases whereas in the case of parallel connection, the current through the array terminals increases. This leads to a change in the position of the maximum power point. The MPP now shifts to a position with higher value of power.

## 1.9 VARIOUS PARAMETERS IN A PV PANEL

A PV panel is characterized by the following factors:

- **Open-circuit Voltage ($V_{oc}$)**

The voltage that appears across the terminals of a PV array when it is open-circuited i.e., no load is connected to its terminals, is termed as the open-circuit voltage of a PV panel. It is 1.11 to 1.25 times the voltage at maximum power point. This voltage increases when the PV panels are connected in series and remains constant in case of parallel connection.

- **Short-Circuit Current ($I_{sc}$)**

  The current that flows through the terminals of a PV array when its terminals are short-circuited is termed as the short-circuit current of a PV panel. It is 1.05 to 1.18 times the current at maximum power point. This current increases when the PV panels are connected in parallel and remains constant in case of series connection.

- **Maximum Power Point:**

  The main objective while generating power from a PV cell is to maximize the generation from it. This requires the array to be operated at its maximum power point. This point is computed such that the product of instantaneous voltage and current here is maximum. These respective voltages and current are termed at voltage at MPP ($V_{mpp}$) and current at MPP ($I_{mpp}$).

- **Fill Factor (FF)**

  Fill factor is a parameter for the determination of the quality of a PV cell. It is the ratio of the product of $V_{mpp}$ and $I_{mpp}$ w.r.t. the product of $V_{oc}$ and $I_{sc}$ as shown in eqn. (1.13).

$$FF = \frac{V_{mpp} I_{mpp}}{V_{oc} I_{sc}} \tag{1.13}$$

Thus, it is the ratio of the area of the rectangle formed by the maximum power point with the voltage and current axes w.r.t. the area of the rectangle formed by the product of $V_{oc}$ and $I_s$ with the voltage and current axes. The closer the value of fill factor to 1,

the better is the quality of the PV cell. A lesser value of fill factor indicates that the cell is a degraded one.

- **Percentage Efficiency**

  Efficiency of a PV array can be determined by the ratio of output power generated by the PV array to the incident power on it. This incident power is a function of the irradiance of the incident light in $W/m^2$ and the operating temperature of the PV array in K. Percentage efficiency can be calculated by multiplying the efficiency with a factor of 100 as depicted in eqn. (1.14).

$$Percentage\ efficiency = \frac{Output\ Power}{Incident\ Power} \times 100 \tag{1.14}$$

## 1.10 MAXIMUM POWER POINT TRACKING (MPPT)

The maximum power point as discussed in the earlier sections, is the point at which if the PV cell operates, it will generate the maximum amount of power. The voltage and current corresponding to this operating point are termed as voltage at maximum power point ($V_{mpp}$) and the current at maximum power point ($I_{mpp}$) respectively. The values of $V_{mpp}$ and $I_{mpp}$ are lower than the open-circuit voltage and short-circuit current of the PV cell. A control system is employed in a PV based system to provide a control action in such a manner that the array operates at the maximum power point.

The maximum power point is a desirable point of operation for the PV array and thus acts as a set point for the MPP tracking system. The robust the controller, the more efficient is the power tracking. It is the time response of the controller i.e., the steady as well as transient response of the controller that distinguishes one controller from one other. Thus, a controller with a stable, transient-free and a faster response with least overshoot and least settling time is desirable for optimal MPP tracking.

## 1.11 EFFECT OF IRRADIANCE & TEMPERATURE ON PV CELL

The working of a PV based system can be affected by various reasons, environmental as well as non-environmental. However, the two main factors which play a major role in determining the course of operation of a PV array are irradiance and temperature. The impact of a change in irradiance is more significantly observed in the current supplied by the PV array ($I_{pv}$) while a change in temperature is observed in the voltage across the PV array ($V_{pv}$). The graphs representing the effect of variation of irradiance as well as temperature for a PV based system designed for 1.5 kW have been represented in Fig. 1.8 (a) and (b) respectively.

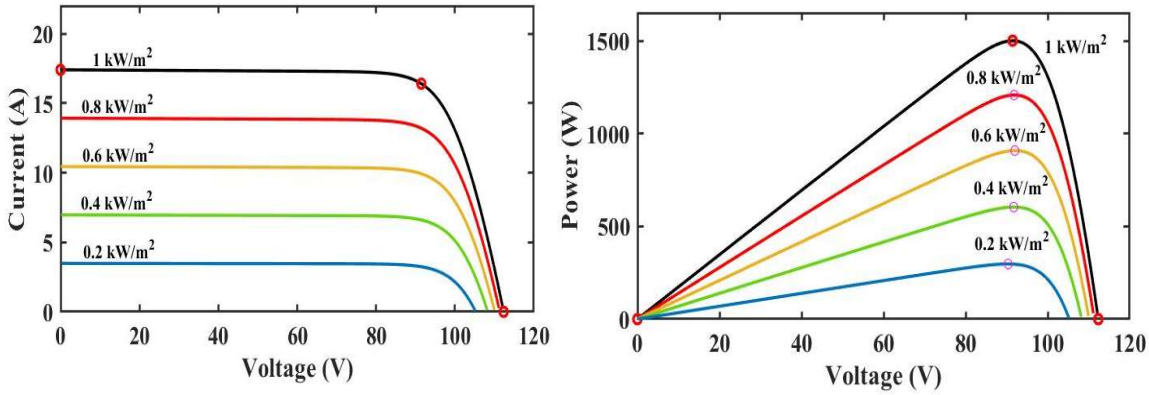


**Fig. 1.8 (a) Effect of Irradiance on I-V and P-V Characteristics of a PV Array**

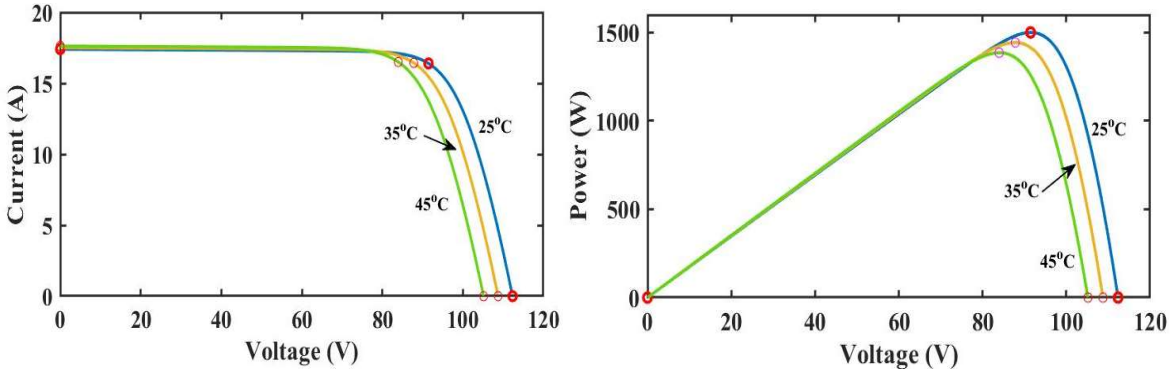


**Fig. 1.8 (b) Effect of Temperature on I-V and P-V Characteristics of a PV Array**

From Fig. 1.8 (a), it can be derived that a reduction in the irradiance causes a reduction in the current generated by the array. Thus, it can be said that the irradiance over the array is directly proportional to the current generated by the PV array. Similarly, in Fig. 1.8 (b), a decrease in temperature leads to a rise in the PV array voltage. Thus, concluding that the temperature and its impact on the PV array voltage are inversely proportional.

## 1.12 DESIGN OF MPPT BASED PV SYSTEM

A PV system consists mainly of a PV array capable of converting the incident radiation into electrical energy. A load is connected to the PV array for utilizing the energy generated by the PV array. A boost converter is also incorporated for impedance matching of the load with the impedance offered by the PV array. The duty cycle of the IGBT switch in the boost converter is continuously altered such that the PV based system operates at the maximum power point. This control action brings in a variation in the duty cycle according to a change in the operating conditions of the PV array. A detailed diagram of the PV based system can be seen in Fig. 1.9.

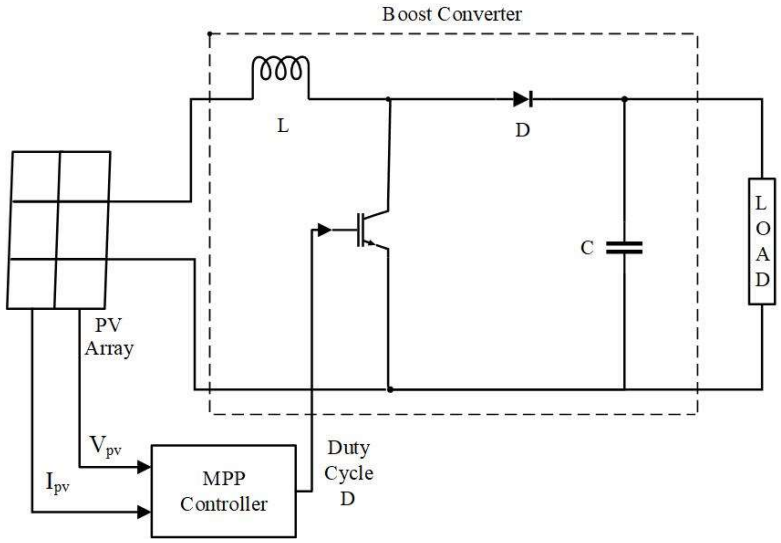


**Fig. 1.9 PV based MPPT system**

These operating conditions could either be based on non-electrical quantities or electrical quantities. Irradiance and temperature fall into the category of non-electrical quantities which could serve as an input for the PV MPPT system. In a similar way, voltage and current act as the electrical inputs for the PV MPPT system. But it is observed that using irradiance and temperature measuring as well as sensing equipment are comparatively more expensive than the ones involving the electrical inputs. Thus, voltage and current in various forms can be utilized for the purpose of MPP operation such as the use of dI/dV ratio or further the dP/dV or dP/dI ratios, which varies from algorithm to algorithm. Many of these algorithms will be discussed and compared in the subsequent sections. The output of the MPPT controller is a change in the duty cycle corresponding to a change in the above discussed ratios.

## 1.13 DESIGN OF BOOST CONVERTER

A boost converter is an essential component in the PV based MPPT system. It is based upon the duty cycle of the boost converter that the entire operation of a PV system depends. The higher the switching frequency, the faster is the switching. The basic circuit diagram of a boost converter includes an inductor, a diode, a capacitor and a switch. An Insulated Gate Bipolar Junction Transistor (IGBT) switch is preferred for this purpose over Bipolar Junction Transistor (BJT) and Metal Oxidized Semiconductor Field Effect Transistor (MOSFET) because of the trade-off it offers between switching power losses and switching frequency. BJT offers low power losses but the switching frequency is significantly low while, MOSFET offers a higher switching frequency but at the expense of higher power losses. Thus, it is required to keep the switching frequency well within limits in order to limit the associated power losses. In this work, a switching frequency of 10 kHz has been selected.

The component design for the boost converter mainly deals with the design of suitable inductance and capacitance for the MPPT operation. Assuming an ideal system with its output power equivalent to its input power, considering a resistive load, the input power and output power for the boost converter can be written as (1.15) and (1.16), respectively.

$$P_i = V_{mpp} I_{mpp} = \frac{{V_{mpp}}^2}{R_{mpp}} \tag{1.15}$$

$$P_o = V_o I_o = \frac{{V_o}^2}{R_o} \tag{1.16}$$

where $V_{mpp}$ and $I_{mpp}$ indicate the desirable input voltage and current respectively i.e., the voltage and current at maximum power point while $R_{mpp}$ refers to the resistance at the maximum power point. For an output resistance of $R_L$, equating the two expressions, we get eqn. (1.17).

$$\frac{V_{mpp}}{V_o} = \sqrt{\frac{R_{mpp}}{R_L}} \tag{1.17}$$

The duty ratio for a boost converter in terms of its input and output voltage can be calculated by eqn. (1.18). Here, since the operation of the array at maximum power is desirable, so the voltage at MPP is taken as the input voltage. Further, the duty ratio can be expressed in the terms of load resistance.

$$D = 1 - \frac{V_{mpp}}{V_o} = 1 - \sqrt{\frac{R_{mpp}}{R_L}} \tag{1.18}$$

According to [15], the optimum value of the load resistance based on the variation of irradiance lies within a limit bound by its value at minimum as well as maximum value of irradiance. This limit is also determined by the desirable range of duty ratio. This optimal value limit has been indicated in eqn. (1.19).

$$R_{L(\min. Irradiance)} \leq R_{L(optimum)} \leq R_{L(\max. Irradiance)} \tag{1.19}$$

Using eqn. (1.18), the expression in eqn. (1.19) can further be written as eqn. (1.20).

$$\frac{R_{mpp(max)}}{(1-D_{min})^2} \leq R_{L(optimum)} \leq \frac{R_{mpp(min)}}{(1-D_{max})^2} \tag{1.20}$$

According to [16], the inductance for a boost converter can be evaluated using (1.21).

$$L = \frac{V_{in} \times D}{\Delta i_L \times f} \tag{1.21}$$

where $V_{in}$ is the input voltage to the boost converter, $i_L$ is the current flowing through the inductor, f is the switching frequency for IGBT switching and D is the duty ratio for the converter. This expression can be modified for the MPPT based system in such a way that for the MPPT purpose, the voltage across the array at MPP is taken as the input voltage and the ripple in the current flowing through the inductor can be taken as the ripple in the current generated by the PV array at MPP. Thus, eqn. (1.21) can be re-written in the terms of current ripple factor $\gamma_{IL}$ to compute the minimum value of inductor as (1.22):

$$L = \frac{V_{mpp} \times D}{\gamma_{I_L} \times I_{mpp} \times f} \tag{1.22}$$

Eqn. (1.22) can further be written in the terms of $R_{mpp}$ as (1.23).

$$L = \frac{R_{mpp}}{\gamma_{I_L} \times f}\left(1 - \sqrt{\frac{R_{mpp}}{R_L}}\right) \tag{1.23}$$

For minimum value of inductance, on equating $(\partial\gamma_{IL}/\partial R_{mpp})$ to zero, the expression for $L_{min}$ is obtained as (1.24).

$$L_{min} = \frac{4}{27}\frac{R_L}{\gamma_{I_L} \times f} \tag{1.24}$$

Similarly, the capacitance value of the capacitive component in the boost converter can be calculated in terms of voltage ripple factor $\gamma_{Vmpp}$ using (1.25).

$$C = \frac{D}{R_L \times \gamma_{V_o} \times f} \tag{1.25}$$

The expression for capacitance in (1.25) can be written in the terms of duty cycle as (1.26).

$$C = \frac{D(1-D)^2}{R_{mpp} \times \gamma_{V_o} \times f} \tag{1.26}$$

Putting the value of D from eqn. (1.18) in eqn. (1.26), we get (1.27).

$$C = \frac{1}{\gamma_{V_o} \times f}\left(\frac{1}{R_o} - \sqrt{\frac{R_{mpp}}{{R_o}^3}}\right) \tag{1.27}$$

The minimum value of capacitance will thus be (1.28).

$$C_{min} = \frac{1}{\gamma V_o \times f}\left(\frac{1}{R_o} - \sqrt{\frac{R_{mpp_{(\min)}}}{{R_o}^3}}\right) \quad (1.28)$$

The inductance and capacitance will however be designed for a 25% greater value than their minimum values in order to ensure a continuous current operation of the converter.

## 1.14 ORGANIZATION OF THE THESIS

This thesis is an effort towards developing optimized AI techniques for MPPT in a designed PV based system. Maximum power point plays a significant role in the operation of a PV based system. MPP operation helps the array to work up to its full potential i.e., the maximum power output it can generate. Thus, maximum power point tracking (MPPT) is employed with the PV arrays to maximize their generation. This thesis includes a discussion about the prevalent conventional techniques and the three main AI techniques i.e., Fuzzy Logic control, Artificial Neural Network (ANN) based control and Adaptive Neuro-Fuzzy Inference System (ANFIS) based control. It is found that ANN has a faster computation speed and thus, a section of the thesis deals with its optimization via the use of the fastest learning algorithm which not only reduces the computation burden but also has a relatively better dynamic response. Further, a simplified and optimized model of a FLC is proposed and developed and it is observed that it outperforms the existing 49 rule FLC, commonly used by researchers as a trade-off between accuracy and computational complexity.

**Chapter 2** contains a brief literature review of the MPP based techniques. It discusses the challenges faced during the partial shading conditions and the contributions of this thesis to the mentioned challenges, mainly the non-linearities introduced due to these conditions.

**Chapter 3** gives an idea about the existing MPPT techniques. The two main discussed techniques are Perturb & Observe (P&O) and Incremental Conductance (InC) technique. The chapter not only discusses their merits but also considers and presents their demerits. Further, the designed system is simulated with the two controllers and based on a comparative

analysis, it is observed that the InC algorithm has a lesser computational time and is relatively more robust.

**Chapter 4** contains a detailed discussion about the requirement of AI techniques and also discusses the three main AI techniques. It contains an in-depth description of their evolution, their structure and the design statements in line with this work. A comparison is drawn between the three and it is found that though ANFIS based controller gives the best results, ANN gives relatively closer results with a faster computational speed.

**Chapter 5** presents an analysis to determine the ANN based learning algorithm that would further optimize the ANN operation. Levenberg Marquardt (LM) algorithm is found to be the optimum learning algorithm. In this chapter, the training as well as performance-based test parameters of the controllers has been discussed in detail.

**Chapter 6** proposes a 4-rule Simplified Optimized Fuzzy Logic Controller (SOFLC). This not only approximates the behavior of a 49-rule conventionally used FLC but also reduces the memory requirement and the computational burden of the controller. A statistical analysis of the simulated controllers is also provided along with their analysis based on the performance indices. This provides an optimized solution for a major challenge of high computational burden faced by the FLCs.

# Chapter 2

# Literature Review

This chapter presents a review starting from the conventional MPPT algorithms and the journey of technologic advancement thereafter leading to state of art technology in MPPT under constant irradiance and strategies to handle partial shading conditions. The growing dominance of artificial (AI) techniques in handling complex control objectives of MPPT of PV array under partial shading environment is also discussed. Based on the available literature, the objectives and scope of proposed work along with author's contribution is presented.

## 2.1 INTRODUCTION

Despite lot of developments in the manufacturing technology of PV and other utilization related aspects, the low energy conversion efficiency is still a bottleneck, due to which the maximum power point tracking (MPPT) of PV array becomes critically important [17]. Another challenge in power generation using PV array is posed by the unpredictable environmental factors [18]. Therefore, the control algorithm of MPPT scheme should be capable enough to address all these issues in order to harness the maximum power from the installed PV arrays.

## 2.2 MPPT-THEN & NOW

Maximum power point tracking is an area of concern when it comes to utilizing the PV based system to its maximum capability [18]. Extensive research has been carried out over the years based on the conventionally used techniques in order to further develop newer, efficient

algorithms using lesser computational time [19]. This has led to deriving the relationship between various parameters of PV array and finding a link between their variation with the variation in the operating power [20]. This forms the basis for most of the existing as well as upcoming algorithms.

The P&O algorithm takes into consideration the variation of power with voltage as the criteria for determining whether the operating point is the MPP [21-25].Thus, the slope of the P-V characteristics plays an important role in order to decide whether the PV array is operating at the maximum power point or away from it and if away, then the sign with the slope gives a clear idea whether the operating point is to the left of the MPP or to its right.

Similar is the case with Hill Climbing method, where the above discussed conditions are determined based on the slope of the P vs. I characteristics of the PV array[26-28].This gives an idea about how a variation in current brings a variation in power.

Incremental Conductance (InC) method on the other hand, considers the incremental change in conductance as a deciding factor for analysing the operating point of the array [29-33]. These conventional techniques are well-known and have been used on priority for their less complexity.

However, over the course of time, it has been observed that the AI based techniques have emerged with a faster convergence and lesser computation time as compared to the conventionally used algorithms and time and again, efforts are being made to further reduce this computational time without hampering the performance of the AI based algorithms [34]. The three main control techniques popularly used as AI techniques are: Fuzzy Logic, Artificial Neural Network and Adaptive Neuro-Fuzzy Inference System (ANFIS) based control. Partial shading is a condition when a section of the array is shaded while the remaining portion receives either uniform irradiance or a different radiation a compared to the shaded portion [35]. This introduces non-linearities in the P-V as well as I-V characteristics of the PV array [36]. AI techniques are well known for their capability of handling the non-linearities in the system [37]. Thus, AI techniques are a suitable choice for the MPP tracking fora PV array during the partial shading conditions.

## 2.3 SCOPE OF WORK AND AUTHOR'S CONTRIBUTION

After reviewing the existing literature, it is observed that extensive research has been carried out on control aspects of MPPT as can be seen in Table 2.1. The control scheme is one of the most important aspects governing the performance of PV array under partial shading conditions. Most of the proposed control algorithms are based on sensing and measurement of voltage and current associated with the PV array.

Conventionally techniques such as Perturb & Observe (P&O), Hill Climbing and Incremental Conductance (InC) Technique are used for effective tracking of maximum power point. The performance of these algorithms may adversely suffer under partial shading scenario. Therefore, it is proposed to explore the AI techniques for efficient MPPT.

AI based control techniques are being used to provide solutions to such ill-defined, nonlinear and complex control problems. AI techniques include the various nature inspired evolutionary algorithms, human intuition and experienced based fuzzy logic controllers, biological nervous system motivated artificial neural networks, genetic algorithm, etc. In this thesis fuzzy logic controllers, ANN, ANFIS controllers and an approximation technique to reduce the complexity of a large rule FLC are explored to enhance performance of PV array operating under partial shading conditions.

**Table 2.1 MPPT Techniques based on the Literature Review**

| Reference | Author | MPPT Technique | Control Variable |
|---|---|---|---|
| [19] | M. Hlaili, H. Mechergui | Variable Step Size Open Circuit Voltage (VSSOCV) | Change in Reference Current |
| [20] | Haider Ibrahim, Nader Anani | Newton-Raphson Method | Change in Duty Cycle |

| | | | |
|---|---|---|---|
| [21] | K.H. Hussein, I. Muta, T. Hoshino, M. Osakada | Golden Section Search with DIRECT algorithm | Change in Duty Cycle |
| [22] | C. Hua, J. Lin, C. Shen | Voltage Feedback Control & Power Feedback Control | Change in Duty Cycle |
| [23] | C. Hua, J. Lin | Voltage Feedback Control & Power Feedback Control | Change in Duty Cycle |
| [24] | N. Femia, G. Petrone, G. Spagnuolo, M.Vitelli | Optimized P&O | Change in Duty Cycle |
| [25] | J. Ahmed, Z. Salam | Improved P&O | Change in Operating Voltage |
| [26] | W. Xiao, W. Dunford | Modified Hill Climbing Method | Switching Duty Cycle |
| [27] | T. Shimizu, O. Hashimoto, G. Kimura | Utility-Interactive Photovoltaic Inverter With Generation Control Circuit | Switching Duty Cycle |
| [28] | A. Ahmed, L. Ran, J. Bumby | Design strategy based on Hill Climbing Method | Change in Duty Cycle |
| [29] | A. Safari, S. Mekhilef | InC with Cuk Converter | Change in Duty Cycle |
| [30] | Q. Mei, M. Shan, L. Liu, J. M. Guerrero | Improved variable step-size incremental-resistance MPPT method | Change in Reference Current |
| [31] | K. Kobayashi, I. Takano, Y. Sawada | Two stage MPPT Control | Change in Inverter Input Voltage |

| | | | |
|---|---|---|---|
| [32] | T. K. Soon, S. Mekhilef | Fast Varying MPP based on InC | Change in Duty Cycle |
| [33] | K. S. Tey, S. Mekhilef | Modified Incremental Conductance MPPT | Change in Duty Cycle |
| [34] | S. Chaudhary, A. Singh | FLC, ANN and ANFIS based MPPT Control | Change in Duty Cycle |
| [38] | R. Alik, A. Jusoh, T. Sutikno | P&O based MPP techniques | Change in Operating Voltage |

Artificial Neural Network models are also modelled and tested. The performance of the ANN models was also observed to be at par with a large rule FLC. Efforts were made to design a lesser complex version with suitable approximation techniques, but the performance did not match the expected response with reduction in complexity of the ANN architecture.

ANFIS model though was performing better than the large rule FLC algorithm as well as ANN by a slight margin but yet the complex structure and large computation time were the main hurdles.

Fuzzy logic controller has come up as a powerful AI tool for handling non-linear and randomly varying operating conditions. The FLCs requires large rule base for precise control, leading to increased complexity of controller. This increased complexity has results in large memory requirement and increased execution time of a specific control action. These limitations provide scope to develop some approximation techniques resulting in less complex solutions (FLCs) without compromising the compensation objectives. The proposed approximation techniques are process-independent and can be implemented to any other complex problem.

The main contributions of the presented work are:

(i) Design and development of simulation model of a Solar PV array under uniform and non-uniform irradiance rigorous simulations are carried out for under randomly varying operating conditions.

(ii) Exploration of ANN and ANFIS models with different algorithms under partial shading operating scenario of PV array. Efforts are also made to approximate their complex models with less complex structures, but the less complex models could not meet the control expectations.

(iii) Design of a 49-rule FLC to provide relatively smooth transition of control action during transient conditions. The simulations results authenticate the design process, with significant improvement in terms of performance indices and other parameters.

(iv) The large rule FLC provides precise control action but has limitation of increased structural complexity leading to large memory requirement, more execution time and slow response. To overcome these issues, less complex optimized simplest fuzzy controllers (SOFLC) is designed, which matches the control performance of a 49-rule FLC but with a reduced and optimized structure.

## 2.4 CONCLUSIONS

This chapter presents an in-depth review covering the brief overview of research, research gaps and their proposed solution. The review summarizes the merits and demerits of the discussed contributions, and provides the guidelines for scope of research and helps in problem formulation.

# Chapter 3

# Conventional MPPT Schemes

This chapter gives an insight into the idea behind conventionally prevalent MPPT based schemes. A complete discussion regarding the algorithms involved in these MPPT techniques has been done along with flowcharts demonstrating the overall working of the algorithm.

## 3.1 INTRODUCTION

The maximum power obtained from a PV array depends upon two main factors i.e., the solar irradiance and the operating temperature of the array. Various maximum power point tracking (MPPT) algorithms are employed in order to obtain maximum output power from the array. The conventionally used MPP techniques include, but are not limited to, Perturb and Observe (P&O), and Incremental Conductance (InC) algorithms.

## 3.2 P&O ALGORITHM

The Perturb and Observe algorithm is the one of the widely used algorithms owing to its easy implementation. In the technique, a small perturbation is introduced in the duty cycle such that the perturbation has to be continued in the same direction if the power increases and reversed if otherwise [38].

At the MPP, the ratio of incremental change in power to the incremental change in voltage i.e. (dP/dV) is equal to zero; towards the left of the MPP, the ratio becomes positive and towards the right of the MPP, it takes a negative value. The P-V characteristic illustrated in

Fig. 3.1 indicates the three regions of operation and their dP/dV ratios. According to the dP/dV ratio, the direction of perturbation to be introduced is determined.

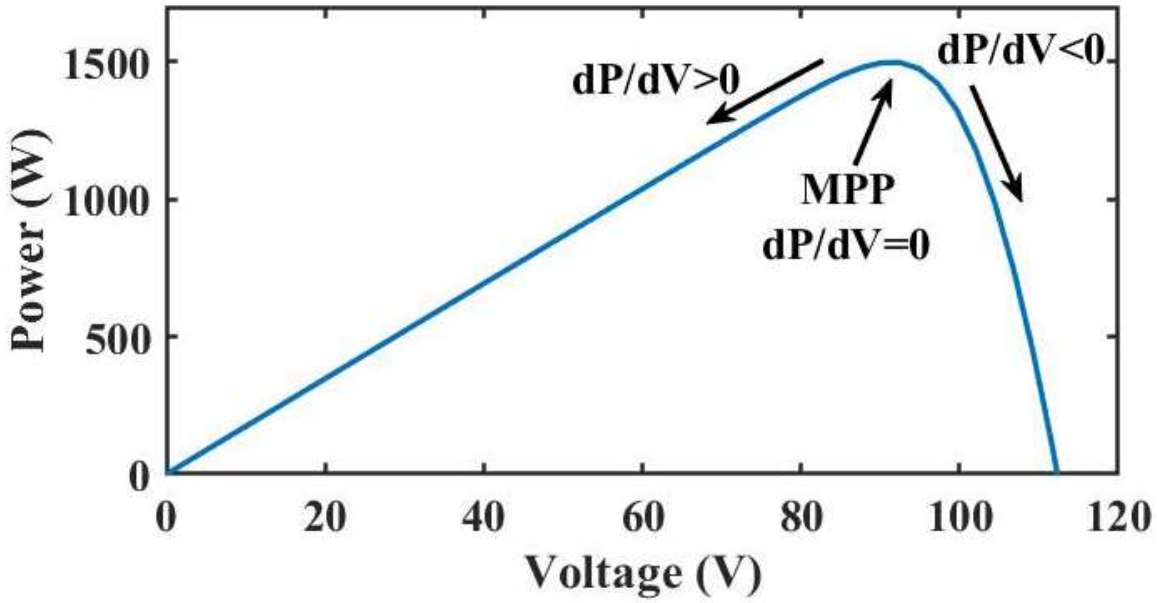


**Fig. 3.1 Operating Regions of P&O MPPT Technique**

The process of perturbation continues until the MPP is reached and the operating point oscillates around it. However, P&O suffers with three main disadvantages: long time for convergence, higher oscillations about the MPP and the drift due to changing irradiance. A flowchart describing the course of perturbation to be introduced according to the algorithm has been depicted in Fig. 3.2.

The voltage across the array and current produced by the array at the present instant are measured and the power at the present instant is computed. Similarly, the power at previous instant is calculated. The difference between the power at the present instant and the previous instant is computed and designated a dP. In a similar manner, the difference between the voltages at the present and previous instant is indicated as dV. If the value of dP at any instant comes out to be zero, then the PV array is assumed to be operating at the maximum

power point. However, if the value of dP is not zero, then the (dP/dV) ratio will determine the nature of perturbation in the duty cycle.

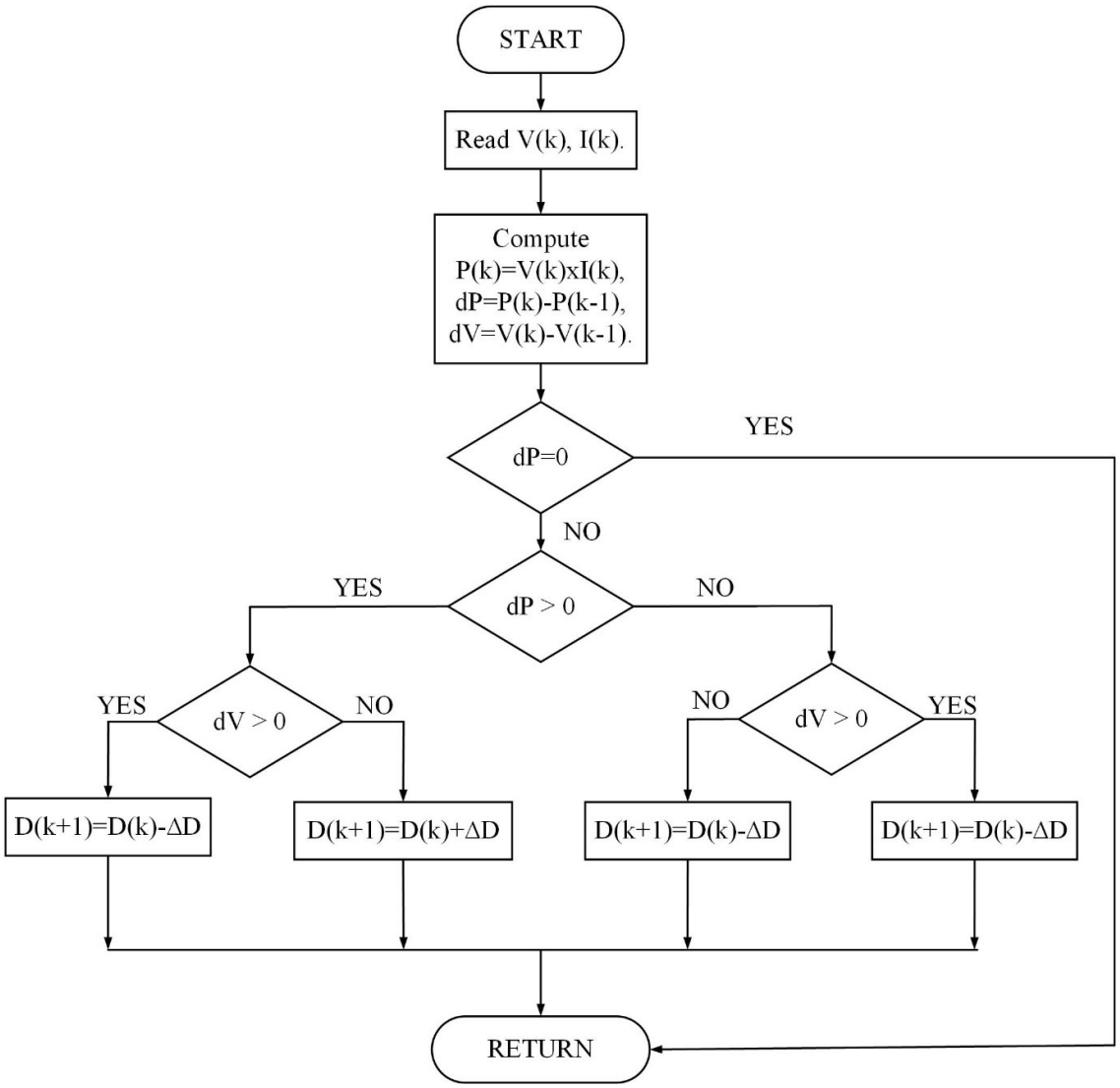


**Fig. 3.2 Flowchart for P&O Algorithm**

The nature of perturbation introduced by the algorithm according to different values of (dP/dV) has been tabulated in Table 3.1.

**Table 3.1 Nature of Perturbation in ΔD according to dP/dV Ratio**

| dP | dV | dP/dV | Nature of Perturbation (ΔD) |
|---|---|---|---|
| + | + | + | - |
| + | - | - | + |
| - | + | - | + |
| - | - | + | - |

The step size for the change in duty cycle i.e., ΔD plays a crucial role in determining the speed of convergence or the time taken by the algorithm to reach the MPP. A higher value of step size leads to a larger fluctuation near the MPP while a smaller value leads to smoother fluctuations.

## 3.3 INCREMENTAL CONDUCTANCE (InC) ALGORITHM

The operation of the Incremental Conductance algorithm is based upon the slope of the P-V characteristics of the array [39]. The slope of the P-V characteristic i.e. (dP/dV) is zero at the MPP.

$$\frac{dP}{dV} = 0 \qquad \text{at MPP} \tag{3.1}$$

$$\frac{dP}{dV} > 0 \text{to the left of MPP} \tag{3.2}$$

$$\frac{dP}{dV} < 0 \qquad \text{to the right of MPP} \tag{3.3}$$

As,

$$\frac{dP}{dV} = \frac{d(IV)}{dV} = I\frac{dV}{dV} + V\frac{dI}{dV} = I + V\frac{dI}{dV} \tag{3.4}$$

Equations (3.1), (3.2) and (3.3) can be written as:

$$\frac{dI}{dV} = -\frac{I}{V} \quad \text{at MPP} \tag{3.5}$$

$$\frac{dI}{dV} > -\frac{I}{V} \quad \text{to the left of MPP} \tag{3.6}$$

$$\frac{dI}{dV} < -\frac{I}{V} \quad \text{to the right of MPP} \tag{3.7}$$

Therefore, the MPP can be tracked by a continuous comparison of incremental conductance (dI/dV) with the instantaneous conductance (I/V). It can also be comprehended as the sum of the former and latter. If the sum of incremental conductance and the instantaneous conductance turns out to be zero, the operating point is considered to be the MPP. However, if the sum turns out to be positive, then the array is considered to be operating to the left of the MPP otherwise, to the right of the MPP as indicated in equations (3.8), (3.9) and (3.10).

$$\frac{dI}{dV} + \frac{I}{V} = 0 \quad \text{at MPP} \tag{3.8}$$

$$\frac{dI}{dV} + \frac{I}{V} > 0 \quad \text{to the left of MPP} \tag{3.9}$$

$$\frac{dI}{dV} + \frac{I}{V} < 0 \quad \text{to the right of MPP} \tag{3.10}$$

The operating regions of the InC algorithm have been shown in Fig. 3.3.

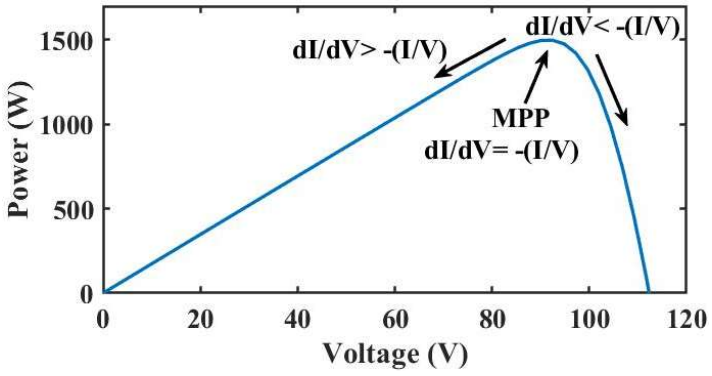


**Fig. 3.3 Operating Regions of InC MPPT Technique**

A flowchart describing the various steps of the InC algorithm has been illustrated in Fig. 3.4. The incremental change in voltage and current i.e. dV and dI can be calculated as the difference between the values of respective quantities at the present and the previous instant.

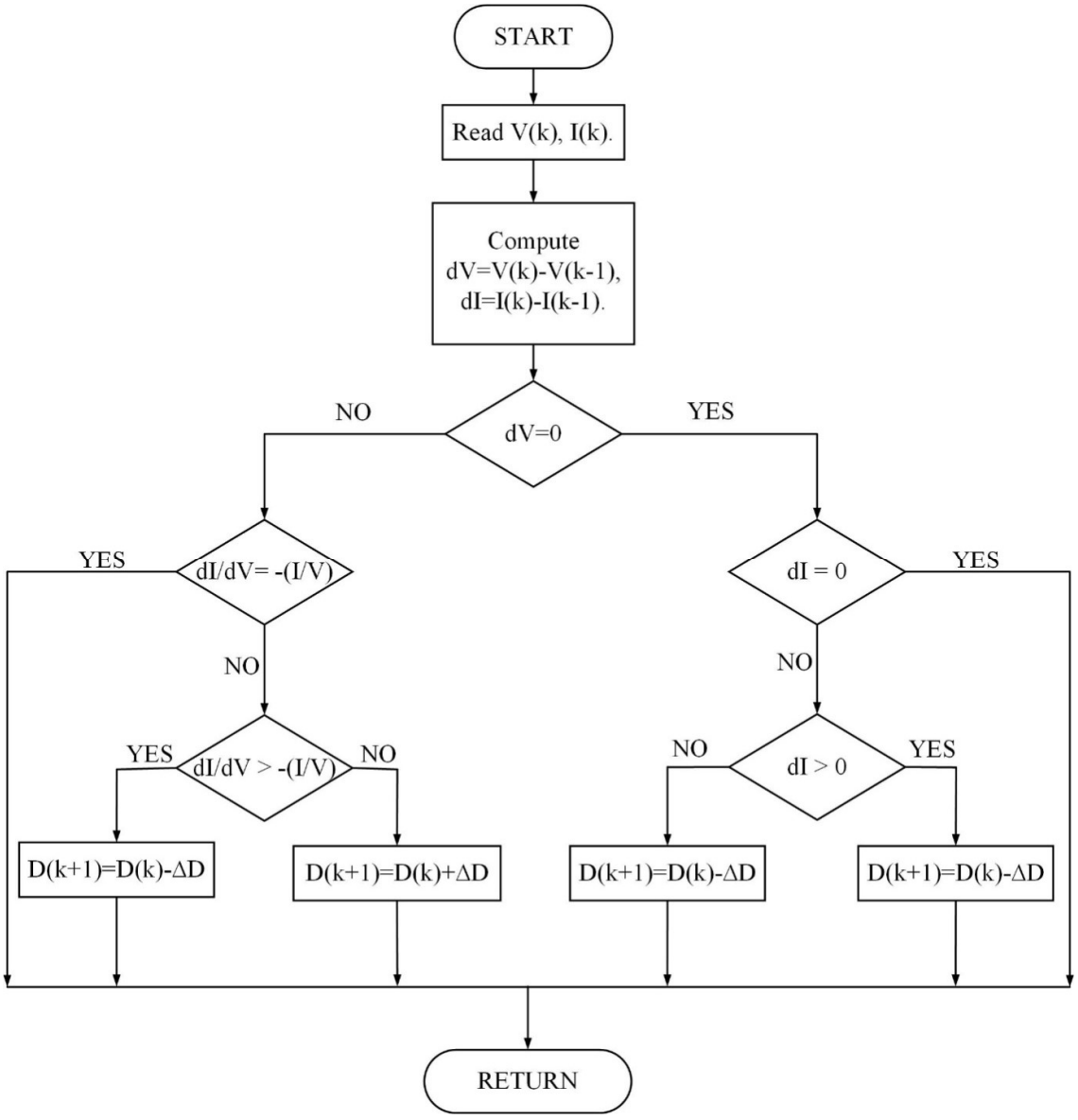


**Fig. 3.4. Flowchart for InC Algorithm**

If there is no incremental change in the voltage as well as current or the sum of incremental as well as instantaneous conductance is zero, then no change in the duty cycle is introduced. However, if the incremental change in voltage is zero but the incremental change in current is

positive, then a negative perturbation is introduced in the duty cycle whereas for a negative incremental change in current, a positive perturbation of the duty cycle comes into picture. In case of a non-zero incremental change in voltage, the sum of incremental and instantaneous conductance acts as a deciding factor for the nature of perturbation in the duty cycle. If the sum is positive, the duty cycle is decremented; otherwise, the duty cycle is incremented.

The InC algorithm can lose track of the MPP in the case of rapid change of irradiance. Due to rapid change in irradiance, the algorithm can even lose track of the MPP [40]. It performs well in the case of step change in irradiance. However, in the case of a change in irradiance in the form of a slope, the algorithm may lose track of the MPP due to a continuous change of the PV curve to be tracked, which in the case of step change, results in an instantaneous change of the PV curve. So, a change in power can be observed not only due to a perturbation in voltage but also because of a change in irradiance. Thus, the detection of the reason behind the change in power is a challenging task for the conventional algorithms.

## 3.4 SYSTEM DESIGN

A PV based system of 1.5 kW has been designed in this work. The arrangement is such that there the PV array contains 6 modules connected in a 3×2 series-parallel configuration. The parameters involved in the designing of the PV array have been tabulated in Table 3.2.

**Table 3.2 PV Array Design Specifications**

| Specification | Rating |
|---|---|
| Maximum Power of each Module | 250.018 W |
| Maximum Power of the Array | 1500 W |
| Open Circuit Voltage ($V_{oc}$) of the Array | 37.45×3 V |
| Short-Circuit Current ($I_{sc}$) of the Array | 8.7×2 A |
| Voltage at MPP ($V_{mpp}$) | 91.84 V |
| Current at MPP ($I_{mpp}$) | 16.32 A |

| | |
|---|---|
| Cells per module | 60 |
| Temperature coefficient of $V_{oc}$ ($K_v$) | -0.32 %/°C |
| Temperature coefficient of $I_{sc}$ ($K_i$) | 0.065 %/°C |
| **Module Specific Parameters** | |
| Light-generated Current ($I_{ph}$) | 8.7072 A |
| Diode Saturation Current ($I_o$) | $6.8168\times10^{-11}$ A |
| Diode Ideality Factor | 0.95037 |
| Shunt resistance ($R_{sh}$) | 406.86 Ω |
| Series resistance ($R_s$) | 0.31177 Ω |

Apart from the PV array design, the design of the boost converter is also a major consideration for the design of a PV based system. The design parameters for the boost converter have been tabulated in Table 3.3.

**Table 3.3 PV Boost Converter Design Specifications**

| Parameter | Rating |
|---|---|
| Operating Frequency | 10 kHz |
| Voltage Ripple Factor | 1 % |
| Current Ripple Factor | 10 % |
| Inductance | 6.3 mH |
| Capacitance | 218 µF |

## 3.5 PARTIAL SHADING

Partial shading conditions occur due to an unexpected shade over the modules during generation of electricity [41]. This could be due to the construction of new buildings or due to the trees near the panel or due to dirt and dust accumulating near the surface of the panel.

This not only reduces the power output of the PV array as a whole but also degrades its performance over time due to the formation of localized hotspots. This is due to the non-linearities introduced in the characteristics of the PV array as depicted in Fig. 3.5.

Such cases are also taken into account during the testing of algorithms to take into consideration, the non-ideal conditions i.e., conditions deviating from the STC which is at an irradiance of 1 kW/m$^2$ for an operating temperature of 298 K. In order to incorporate these cases, the PV system is designed using PV panels receiving variable irradiances. The irradiances given to the module are in accordance to their position in the array matrix. For example, the module in the first row as well as column will receive an irradiance of $Irr_{11}$. Likewise, the module in the third row as well as second column would receive an irradiance of $Irr_{32}$. Such an arrangement has been shown in Fig. 3.6.

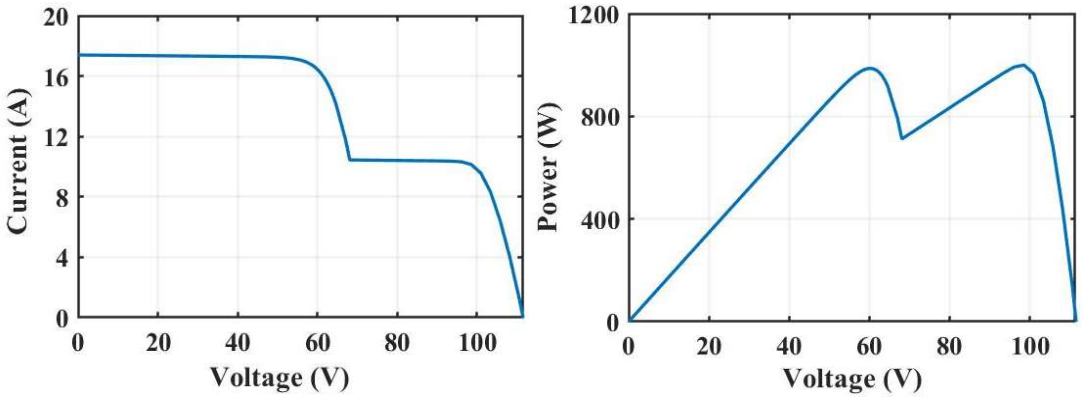


**Fig. 3.5. Effect of partial shading on I-V and P-V characteristics of PV array**

Multiple test cases of uniform as well as non-uniform irradiance have been considered. For simplicity, four test cases have been considered. These can be classified as STC, top shading, patch shading as well as bottom shading. The STC case represents an irradiance of 1 kW/m$^2$ at a temperature of 298 K. Since partial shading is being considered, so a variation in temperature is avoided and hence, the designed system has been tested for all the cases assuming a constant temperature of 298 K.

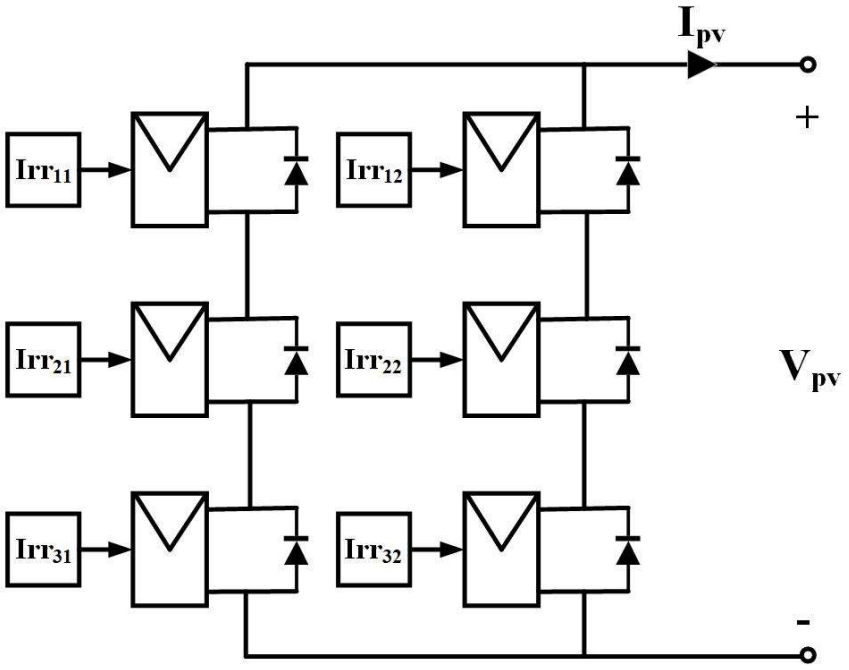


**Fig. 3.6 PV array irradiance arrangement for the designed system**

For the three cases of partial shading, eqns. (3.11), (3.12) and (3.13) will hold true since the cases are related to a horizontal configuration of system.

$$Irr_{11} = Irr_{12} = Irr_1 \tag{3.11}$$

$$Irr_{21} = Irr_{22} = Irr_2 \tag{3.12}$$

$$Irr_{31} = Irr_{32} = Irr_3 \tag{3.13}$$

The variation in Irr1, Irr2 and Irr3 has been shown in Fig. 3.7.

In the second test case i.e., top shading, an irradiance of 0.9 kW/m$^2$ is incident upon the first and second row of the modules while a uniform irradiance of 1 kW/m$^2$ is incident upon the third row of the modules i.e., $Irr_1$= $Irr_2$= 0.9 kW/m$^2$ and $Irr_3$=1 kW/m$^2$. Similarly, in the third test case, patch shading with an irradiance of 0.4 kW/m$^2$ on the intermediate row of the modules has been taken into account i.e., $Irr_2$ = 0.4 kW/m$^2$ and $Irr_1$= $Irr_3$=1 kW/m$^2$ while the fourth case includes the shading of the bottom set of modules with an irradiance of 0.25 kW/m$^2$ i.e., $Irr_1$ = 1 kW/m$^2$ and $Irr_2$= $Irr_3$=0.25 kW/m$^2$.

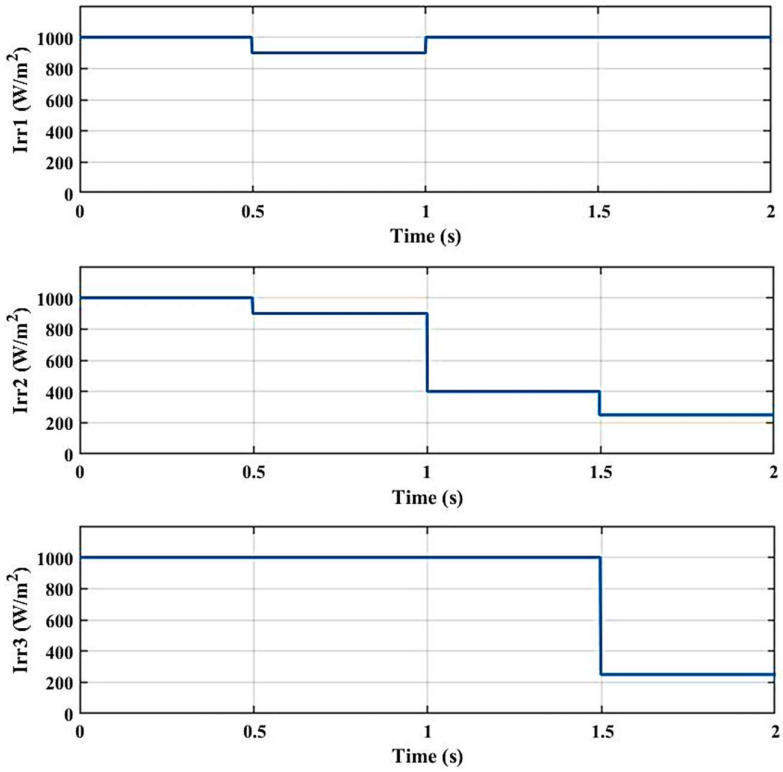


**Fig. 3.7 Variation of Irradiance in the four test cases**

The P-V and I-V characteristics obtained for the above discussed test case have been illustrated in Fig. 3.8. The LMPPs and GMPPs have further been marked in Fig. 3.8.

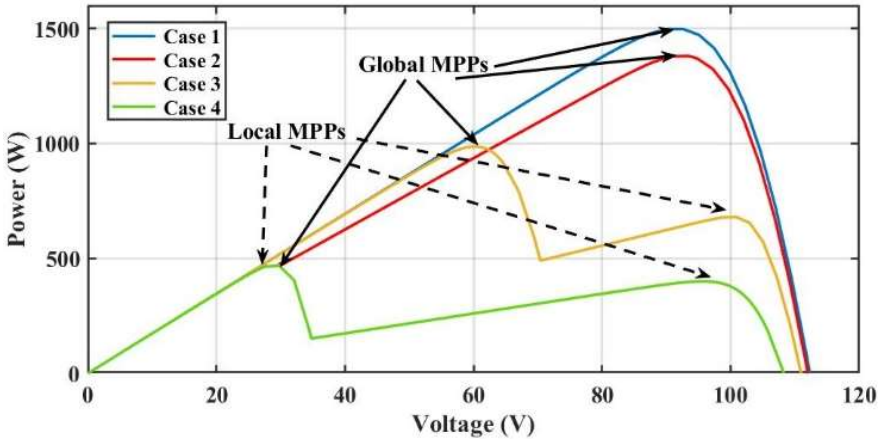


**Fig. 3.8 P-V & I-V characteristic of the designed array under the four test cases**

## 3.6 PERFORMANCE ANALYSIS OF P&O AND InC ALGORITHMS

Based on the designed PV system with corresponding irradiance patterns, the performance of P&O and InC algorithms is compared. On applying the irradiance inputs discussed in the previous section, the response for the designed PV array is obtained and can be observed in comparison with the AI based controllers in the upcoming section.

Meanwhile, a comparison of the P&O and InC algorithms has been done using some basic parameters such as power tracked, settling time, tracking efficiency and computation time in Table 3.4 and 3.5 respectively.

Thus, it can be seen that the even though the tracked power in P&O and InC is nearly same, there still exists a difference in their performance with settling time and tracking efficiency as the basis. The wide disparity in their computational times significantly proves that InC is a better controller.

**Table 3.4 Comparative analysis of P&O and InC algorithm**

| | Control Technique | Power Tracked (W) | Settling Time | Tracking Efficiency (%) |
|---|---|---|---|---|
| **Test Case-1** | **P&O** | 1519 | 0.032 | 98.73 |
| | **InC** | 1521 | 0.034 | 98.6 |
| **Test Case-2** | **P&O** | 1398 | 0.022 | 98.69 |
| | **InC** | 1395 | 0.0203 | 98.91 |
| **Test Case-3** | **P&O** | 997.4 | 0.131 | 98.92 |
| | **InC** | 997.7 | 0.131 | 98.89 |
| **Test Case-4** | **P&O** | 475.3 | 0.132 | 98.96 |
| | **InC** | 474.3 | 0.127 | 99.17 |

**Table 3.5 Comparative analysis Computational Time of P&O and InC algorithm**

| Control Technique | Computation Time (s) |
|---|---|
| **P&O** | 726.57 |
| **InC** | 241.21 |

## 3.7 CONCLUSIONS

Perturb & Observe as well as Incremental Conductance are two conventionally used techniques. They are widely used for the low complexity MPPT solution they offer. Based on the simulated results, it is found that InC takes a smaller computational time.

# Chapter 4

# AI based MPPT Techniques

## 4.1 INTRODUCTION

Irradiance and temperature play a key role in determining the performance of a PV array. In the case of uniform irradiance, the P-V characteristics of the PV array consist of only one peak i.e., at the maximum power point. However, the irradiance conditions may not always remain uniform. Partial shading of the PV array may occur when the light incident at different locations of the PV array does not reach the panels due to various factors such as clouds passing by, shade due to adjacent buildings or trees [42].

Due to the phenomenon of partial shading, not only does the power output of the array reduces but there is also an introduction of multiple peaks in the PV characteristics of the array. Among the multiple peaks, the peak with the overall maximum power is termed as the Global Maximum Power Point (GMPP) while remaining peaks are termed as Local Maximum Power Points (LMPPs) [43]. This introduction of multiple power peaks in the PV characteristics introduces non-linearities in the system, which are to be taken care of by the MPPT controllers.

Thus, the array may operate at a point which is not characterized by the global maximum power. This will lead to a decrement in the output power compared to the actual power that could have been generated by the array. Bypass diodes are used to reduce the impact of shaded PV cells serving as hotspots while in reverse biased mode [44].

## 4.2 FUZZY LOGIC CONTROL

Fuzzy logic is an area of artificial intelligence that deals with reasoning algorithms that are employed in robots to mimic human thinking and decision making. The fuzzy logic controller (FLC) is a fuzzy logic-based controller that converts a linguistic control strategy based on expert knowledge into an automatic control strategy. The main idea behind this unique control paradigm is to design controllers intuitively using the knowledge and expertise of the human operator. Control, image processing, signal processing, approximation, modeling, and other technical applications have all benefited from fuzzy set theory. Fuzzy control, on the other hand, is the most successful and active field. The fuzzy logic control has a number of advantages over traditional control [45]:

(i) the mathematical model of the system to be controlled is not required.

(ii) A good non-linear controller can be created without sophisticated mathematics.

(iii) FLCs can deal with nonlinearity and uncertainty in control systems without having to rely on mathematical models.

### 4.2.1 Evolution of Fuzzy Logic Control

Since Zadeh [46] proposed fuzzy set theory as a new way to express the ambiguous and inexact nature of the real world in 1965, research on the theory and use of fuzzy logic has been going on. It has been proved to be a valuable tool in dealing with uncertainties and non-linearities in control systems, among its numerous applications. Fuzzy control has been applied in a variety of industrial applications during the last few decades.

Thus, fuzzy logic is a strategy for dealing with inaccurate, unclear, or "fuzzy" information found in power systems. The phrase "fuzzy logic" has been applied in two ways. Fuzzy logic is a logical system that generalizes traditional two-valued logic, which is a multi-valued logic extension for reasoning under uncertainty. In a broad sense, fuzzy logic is the theory of fuzzy sets as a generalization of ordinary set theory, with graded membership and soft boundaries

[47]. The fact that practically all natural classes and notions are fuzzy rather than crisp gives rise to fuzzy set theory. With the use of linguistic variables and membership functions, fuzzy logic systems provide an ideal foundation for modeling uncertainty and imprecision in human thinking.

For dealing with the heuristics of linguistically stated algorithms, fuzzy theory is a sophisticated as well as apt tool. These linguistic algorithms are basic, easy-to-understand natural language expressions that represent expert knowledge obtained from years of experience by human experts and operators. Furthermore, only a few of these statements are required to adequately describe complicated processes [48]. These natural language assertions can be categorized into the following categories:

(i) Deterministic linguistic term (Singleton)

(ii) Crisp linguistic term (Crisp sets)

A deterministic linguistic phrase, also known as a singleton, is a natural language statement that is used to express an element or variable that has only one interpretation. Natural language expressions sometimes refer to a range of values rather than a single value. A crisp linguistic phrase or crisp set is the collection of all values in that interval (range). In everyday life, it is quite usual to utilize intuitive natural language statements that convey some level of uncertainty. Fuzzy notions are used to mediate and communicate information, ideas, and understanding. Membership functions (MFs) with a membership value in the interval [0, 1] characterize such claims. Fuzzy linguistic terms or fuzzy sets are the names given to these uncertain yet precise statements.

A fuzzy set is a set with variable bounds, as defined by fuzzy theory. Membership values in the interval [0, 1] are used to express the items of this set. Elements of fuzzy sets, unlike those of traditional sets, do not have to meet all of the set's attributes in order to be a member. The fuzzy set converges on the conventional set in the limiting scenario. The membership value ‘zero' for an element indicates that it is completely absent from the fuzzy set, whereas the value ‘one' indicates that it is fully included. A fuzzy set introduces ambiguity by removing the sharp line that separates group members from non-members. As a result, rather

than being abrupt, the transition from full membership to non-membership is gradual. As a result, fuzzy sets can be thought of as a broadening and expansion of crisp set concepts; nonetheless, some theories are unique to the fuzzy framework.

### 4.2.2 Definition of Crisp and Fuzzy sets

In a universe of discourse, a set is defined as universal set X. The relationship between a crisp set A and a universal set X is represented as (4.1).

$$A \subseteq X \quad (4.1)$$

If an element x is contained in the set A, it is termed a member of the set A, as shown in (4.2).

$$x \in A \quad (4.2)$$

Set A with the elements $a_1$, $a_2$,....an as the members of the set is depicted in (4.3).

$$A = \{a_1, a_2 \ldots . a_n\} \quad (4.3)$$

To express whether an element x is contained in a set A, membership functions are utilised. As a result, the membership function is defined in eqn. (4.4) and (4.5).

$\mu_A(x) = 1$ if and only if $x \in A$ , and (4.4)

$\mu_A(x) = 0$ if and only if $x \notin A$ (4.5)

Each member of the universal set is assigned a value of 0 or 1 using the membership function of a crisp set. The membership function, in other words, maps elements from the universal set X to the set {0, 1} which can be written as (4.6).

$$\mu_A : X \to \{0,1\}, \ \forall x \in X \quad (4.6)$$

The theory of fuzzy sets can be applied when there is an unclear border. In such a case, the membership function maps each element in a fuzzy set to a real number between 0 and 1 as in (4.7).

$$\mu_A : X \rightarrow [0,1], \ \forall x \in X. (4.7)$$

The probability that an element belongs to set A is indicated by the value allocated to it.

### 4.2.3 Membership Functions

A membership function is a shape created by all of the membership degrees associated with a fuzzy collection (MFs). A membership function (MF) is a curve that specifies how each point in the input space is converted to a membership value (or degree of membership) between 0 and 1. The membership distribution does not always vary linearly with the universe of discourse. As a result, we have a variety of membership distributions known as membership functions. Triangular, trapezoidal, sigmoid, exponential, and bell shaped MFs are examples of different forms of MFs.

These MFs can be represented either graphically or functionally. The functional form of MF is better suitable for simulations utilizing fuzzy logic tools since it can be changed using fuzzy arithmetic. Straight lines are used to create the most basic membership functions. The triangle membership function is the simplest of them. It is a triangle formed by connecting three points.

The trapezoidal membership function has a flat top and is essentially a truncated triangle curve, which is a subset of the triangular membership function. The advantage of these straight-line membership functions is their simplicity. As a result, these two membership functions are the most widely employed. The functional description of these functions has been represented in (4.8) and (4.9), respectively.

**i) Triangular function**

$$\mathrm{T}(x;\mathrm{a},\mathrm{b},\mathrm{c}) = \begin{cases} 0 & \text{for } x < \mathrm{a} \\ (x-\mathrm{a})/(\mathrm{b}-\mathrm{a}) & \text{for } \mathrm{a} \le x \le \mathrm{b} \\ (\mathrm{c}-x)/(\mathrm{c}-\mathrm{b}) & \text{for } \mathrm{b} \le x \le \mathrm{c} \\ 0 & \text{for } x > \mathrm{c} \end{cases} \quad (4.8)$$

where a, b and c form the vertices of the triangular membership function as shown in Fig. 4.1 (a).

**ii) Trapezoidal function**

$$T(x;a,b,c,d)=\begin{cases}0 & \text{for } x\le 0\\ (x-a)/(b-a) & \text{for } a\le x\le b\\ 1 & \text{for } b\le x\le c\\ (d-x)/(d-c) & \text{for } c\le x\le d\\ 0 & \text{for } x\ge d\end{cases} \tag{4.9}$$

where a, b, c and d form the vertices of the trapezoidal membership function as shown in Fig. 4.1 (b). A graphical representation of triangular and trapezoidal functions has been shown in Fig. 4.1 (a) and (b) respectively.

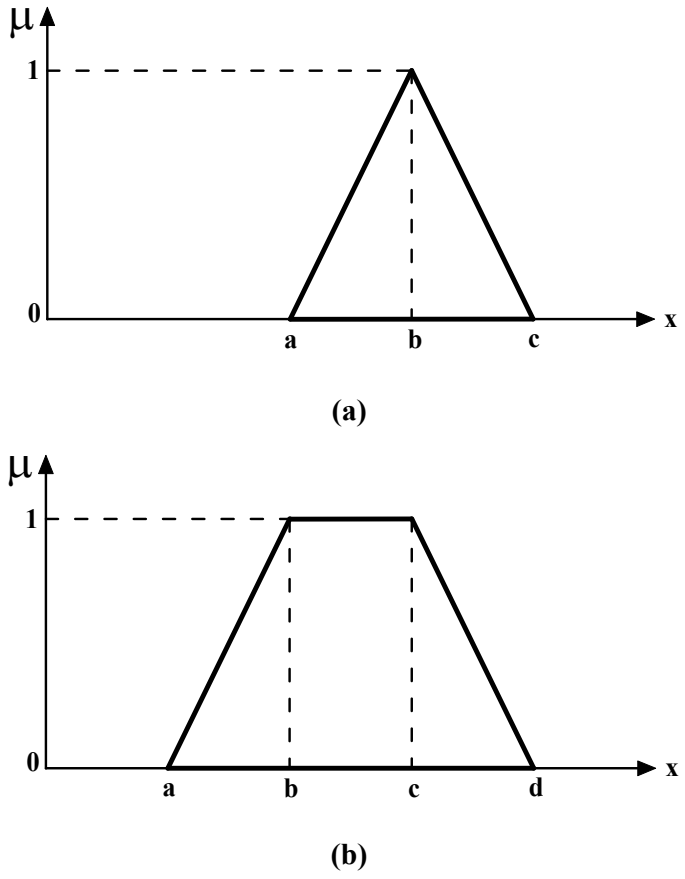


**Fig. 4.1 (a) Triangular function, and (b) Trapezoidal function**

### 4.2.4 Basic Structure of a Fuzzy Logic Controller

Figure 4.2 depicts the basic setup of a fuzzy logic controller (FLC). A fuzzy logic system, in general, maps crisp input into crisp output by an intermediary conversion in fuzzy values known as membership functions. It consists of three main modules:

(i) Fuzzification

(ii) Knowledge Base and Inference engine

(iii)Defuzzification

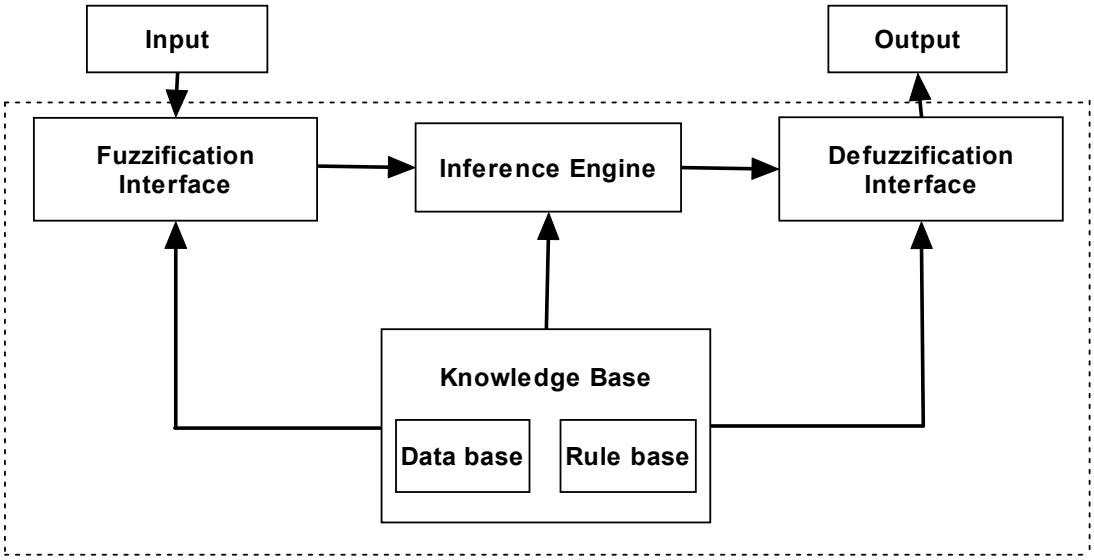


**Fig. 4.2 Basic structure of a fuzzy logic based controller**

Fuzzification transforms input data into linguistic values that can be used as fuzzy set labels. An FLC's knowledge base is made up of two parts: a data base and a rule base. The database contains the definitions that are required for language control rules and fuzzy data. The conditional assertions that make up fuzzy logic are expressed using if-then rule statements. All of these statements are gathered into a rule base. Instead of a precise mathematical model, the rules are a set of linguistic statements based on expert knowledge, including experience and heuristics.

Fuzzy logic principles are employed in the fuzzy inference engine to combine fuzzy rules into a mapping from fuzzy input sets to fuzzy output sets. Membership functions, fuzzy logic operators, and if-then rules are all used in the fuzzy inference process. Fuzzy rule-based inference can be thought of as an interpolation system in mathematics since it allows the fusion of many fuzzy rules when their requirements are all met to some extent. The fuzzy set that is the output of the inference engine is defuzzified to produce a crisp output. The subsections that follow provide a more detailed explanation of these modules.

#### 4.2.4.1 Fuzzification

The fuzzy controller's interpretation of input crisp data is known as the fuzzification process. It is made up of two primary parts:

(i) Labels

(ii) Membership functions

The membership function is the function that connects a number to each element x of the universe (x). In crisp set theory, an element is either a member of or not a member of a set. Many degrees of membership (between 0 and 1) are allowed in fuzzy set theory. As a result, a fuzzy set A is associated with a membership function A(x), which transfers every element of the universe of discourse X to the interval [0, 1].

A fuzzy logic controller collects input data, also known as the fuzzy variable, and analyses it using user-defined membership functions during fuzzification. To some extent, every element in the world of discourse is a member of a fuzzy set, which may be zero. A fuzzy set such as negative, positive, and so on is described by the degree of membership for all of its members. Based on how well the input data fits into each membership function, the controller assigns it a degree in the range [0, 1]. There are numerous membership functions that can be applied to each fuzzy controller input. Each membership function has its own name, which is referred to as a label.

#### 4.2.4.2 Knowledge Base and Inference Engine

The controller evaluates the input data, as defined by the membership functions, to arrive at a control output during fuzzy processing. The processor performs two tasks during this stage:

(i) Rule assessment

(ii) Calculation of Fuzzy Outcomes

Rule evaluation is based on the idea that most complex problems are made up of a series of simple problems that can be solved quickly. Fuzzy logic employs an inference process made up of IF-THEN statements, each of which provides a response. A rule is activated or triggered when an input condition meets the IF section of the rule statement. When the IF section of the rule is activated, a control output is generated based on the THEN part of the rule statement.

Many rules may exist in a fuzzy logic system, each of which corresponds to one or more IF conditions. A rule can contain many input criteria that are logically linked in an AND or OR relationship to trigger the rule's conclusion. In a fuzzy control process, more than one rule may be triggered at the same time. The controller in this example examines all of the rules to arrive at a single outcome value before moving on to the defuzzification phase.

#### 4.2.4.3 Defuzzification

The defuzzification method used to generate the output corresponding to each label determines the fuzzy controller's ultimate output value. The controller turns the fuzzy output into crisp data during defuzzification. As a result, defuzzification is the conversion of a fuzzy set to a single crisp value. It's the reversal of the fuzzification process. Defuzzification can be accomplished in a number of ways. In fuzzy control, the following defuzzification strategies have been widely used:

1. Centre of gravity method

2. Mean of maxima method

3. Centre of sums

#### 4.2.4.3.1 Centre of Gravity method

The centroid or centre of area defuzzification method is also known as the centre of gravity defuzzification method. It is the most often used defuzzification approach since it yields an accurate result by combining the weighted values of many output membership functions. The weighted average of the elements in the support set is the defuzzified value. For a continuous membership function, the crisp output value [49], say x*, is written as (4.10).

$$x^* = \frac{\int \mu(x).xdx}{\int \mu(x)dx} \tag{4.10}$$

For a discrete membership function, however, the integration is substituted with summation, as shown in (4.11).

$$x^* = \frac{\sum_{i=1}^{n} \mu(x_i).x_i}{\sum_{i=1}^{n} \mu(x_i)} \tag{4.11}$$

where n is the number of samples, $x_i$ denotes the elements, and $\mu(x_i)$ denotes the value of membership.

Although its computing complexity is very high, the centroid method of defuzzification is a widely used method.

#### 4.2.4.3.2 Mean of Maxima method

Choosing the point with the most possibilities, i.e., maximal membership, is an intuitive method. On the rule output with the highest membership function grade, the maximum value

defuzzification method is used to determine the final fuzzy output value. When many such points exit, it is a usual practice to pick the mean of the maxima (MOM). Discrete output membership functions are the most common application for this technology. In this situation, the defuzzified output is given by (4.12).

$$x^* = \frac{\sum_{x_i \in \mathrm{M}}^{n} x_i}{|\mathrm{M}|} \tag{4.12}$$

where, M={ $x_i \mid \mu(x_i)$ is equal to the height of fuzzy set}

#### 4.2.4.3.3 Centre of Sums method

In the centroid technique, the overlapping area is only considered once, however in the centre of sums (COS) method, the overlapping area is calculated twice. In this situation, the defuzzified output x* is given by (4.13).

$$x^* = \frac{\sum_{i=1}^{N} x_i \sum_{k=1}^{n} \mu_{\mathrm{A_k}}(x_i)}{\sum_{i=1}^{N} \sum_{k=1}^{n} \mu_{\mathrm{A_k}}(x_i)} \tag{4.13}$$

where, the number of fuzzy sets is n, while the number of fuzzy variables is N.

This approach is also popular because of its ease of use and quick inference cycles.

### 4.2.5 Control Scheme of FLC based MPPT of PV Array

The slope of a P-V characteristics is employed as error (e) in the suggested fuzzy control method, and change in error (e) is evaluated by subtracting error at the instant prior to the present from the error at the present instant of time, as illustrated in (4.14) and (4.15):

$$e(k) = \frac{\Delta P(k)}{\Delta V(k)} \tag{4.14}$$

$$\Delta e(k) = e(k) - e(k-1) \tag{4.15}$$

The FLC produces incremental duty cycle (D) change as its output. As illustrated in Fig. 4.3, the duty cycle is continuously regulated by this gradual change in duty cycle.

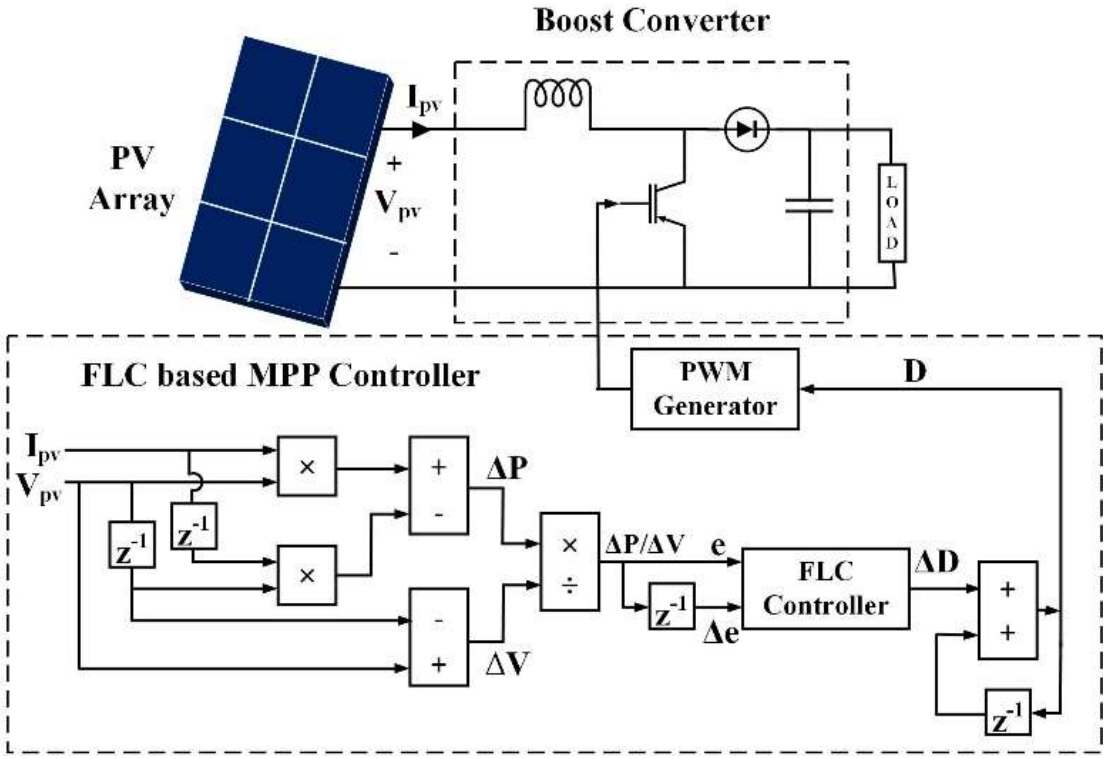


**Fig. 4.3 Fuzzy Logic Control Scheme**

### 4.2.6 Fuzzy Rule Base Design

In the designed fuzzy logic controller, a uniform division of the universe of discourse in seven levels is considered. These seven levels are:

- NL (negative large)
- NM (negative medium)
- NS (negative small)
- ZE (zero)
- PS (positive small)
- PM (positive medium)
- PL (positive large)

Triangular membership functions are used owing to their simplicity. The inputs i.e., e and Δe and the output ΔD are mapped to these seven levels known as the membership functions. Thus, for seven possibilities of the membership function of the first input variable and similar seven possibilities of the membership function of the second input variable, there will be a total of 49 (7×7) possibilities for the output variable. Thus, the membership function plot of the designed FLC can be represented as Fig. 4.4.

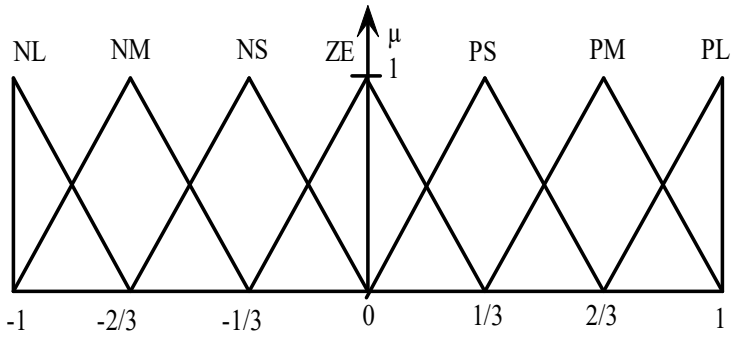


**Fig. 4.4 Triangular Membership Function for the designed FLC**

Based on the knowledge of the variation in parameters with a change in the corresponding input parameters, a 49-rule base is designed as shown in Table 4.1.

**Table 4.1 49-rule base for the designed FLC**

| **e/ Δe** | **NL** | **NM** | **NS** | **ZE** | **PS** | **PM** | **PL** |
|---|---|---|---|---|---|---|---|
| **NL** | PL | PL | PM | PL | PM | PL | PL |
| **NM** | PL | PM | PS | PM | PS | PM | PL |
| **NS** | PM | PS | PS | PM | PS | PS | PM |
| **ZE** | ZE | ZE | ZE | ZE | ZE | ZE | ZE |
| **PS** | NM | NS | NS | NM | NS | NS | NM |
| **PM** | NL | NM | NS | NM | NS | NM | NL |
| **PL** | NL | NL | NM | NL | NM | NL | NL |

Table 4.1 can, for instance, be comprehended as:

For a NL i.e., negatively large error, e and a NS (negatively small) change in error Δe, the response of the system i.e., ΔD should be PM (positively medium).

Similarly, for a PM value of error and a PL value of change in error, the response would be NL i.e., negative large.

## 4.3 ARTIFICIAL NEURAL NETWORKS (ANN) BASED CONTROL

The functioning of an ANN can be compared to that of the human brain. The human brain is a complicated, non-linear machine that uses parallel computing [50]. It gains the ability to modify the basic structure of the neurons over time, to conduct specific computations, and to make decisions based on those computations. An artificial neural network (ANN) is a system that mimics how the brain does a specific task. It attempts to emulate the organic nervous

system and displays key features such as learning, fault tolerance, and non-linear problem solving.

An artificial neural network is trained using a dataset that includes the output parameters as well as the intended target values. For a subset of the dataset, the neural network is tested and validated. Due of its ability to generalize, the ANN can predict the output for the new dataset, or another subset of the dataset it was not trained for, based upon its past learning experience.

ANNs have features that help it succeed, such as simplicity and a quick response time. They do not require detailed system information. They read and examine the system's past data and correlate the system's behavior with previously registered information to identify and assess the relationship between inputs and outputs. Additionally, NNs can deal with nonlinear systems and operate with numerical or analog input, are reasonably significant in terms of generating the best answers, and the user does not require basic mathematical understanding.

### 4.3.1 Basic Structure of an Artificial Neural Network (ANN)

The multiprocessor computing systems used by ANNs are diverse. It is made up of a number of very basic and highly interconnected processors known as neurons, which are analogous to biological neurons in the brain. A neuron is a data-processing unit that is essential for a neural network's functionality. Fig.4.5 shows the fundamental model of a single neuron, where x is the input vector, w, the weight vector of the connection, b is the bias, Φ, represents the activation function, and y is the output vector.

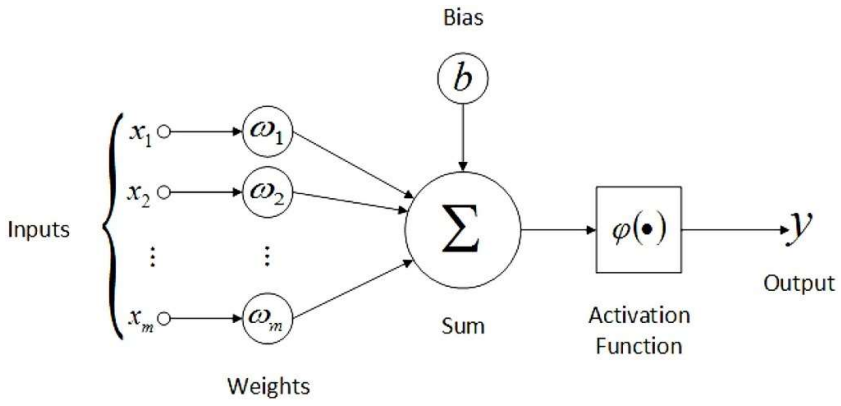


**Fig. 4.5 Basic Structure of a Neuron**

The output of the neuron based on the basic structure of a neuron can be computed as (4.16).

$$y_k = \emptyset\left(\left(\sum_{k=1,j=1}^{n,m} w_{kj}x_j\right) + b_k\right) \tag{4.16}$$

The basic structure of an ANN includes three main modules:

**1. Synaptic links:**

Each synapse, or connecting link, has its own weight or strength. In particular, the synaptic weight $w_{kj}$ is multiplied by a signal $x_j$ at the input of synapse j connected to neuron k. The subscripts of the synaptic weight $w_{kj}$ must be written in a specific order. The first subscript in $w_{kj}$ refers to the neuron in question, while the second subscript refers to the weight's input end of the synapse. The synaptic weight possessed by an artificial neuron can fluctuate from negative to positive.

**2. Adder:**

The processes described here comprise a linear combiner; an adder for adding the input signals, weighted by the different synaptic strengths of the neuron.

**3. Activation Function:**

An activation function limits the magnitude of a neuron's output. The activation function is also known as a squashing function since it reduces the output signal's allowable amplitude range to a fixed value.

### 4.3.2 Activation Functions

Activation functions are an important element of a neural network's architecture. The hidden layer activation function determines how successfully the network ANN based model learns the dataset with which the ANN is trained. The type of predictions the model may produce is determined by the activation function used in the output layer. Fig. 4.6 represents the various type of activation functions.

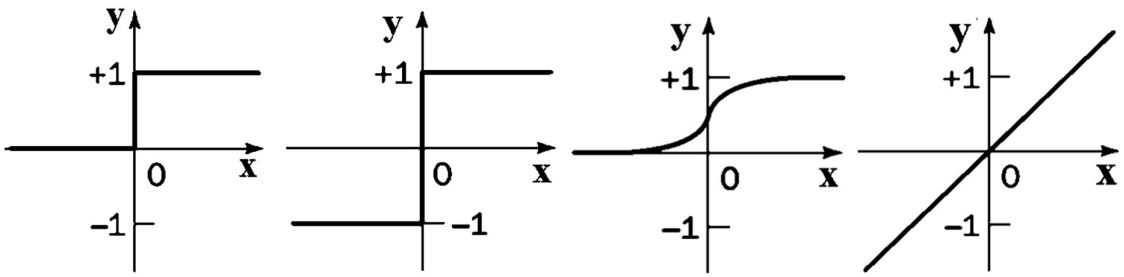


**Fig. 4.6 Activation functions (a) Step function (b) Sign function (c) Sigmoid function (d) Linear function**

The mathematical representation of various activation functions is as follows:

- **Step Function**

$$y = \begin{cases} 1, & if\ x \geq 0 \\ 0, & if\ x < 0 \end{cases} \tag{4.17}$$

- **Sign Function**

$$y = \begin{cases} 1, \ if \ x \geq 0 \\ -1, \ if \ x < 0 \end{cases} \quad (4.18)$$

- **Sigmoid Function**

$$y = \frac{1}{1+e^{-x}} \quad (4.19)$$

- **Linear Function**

$$y = x \quad (4.20)$$

### 4.3.3 Multilayer Perceptron Model

Input layer, hidden layers, and output layer make up the multilayer perceptron model of ANN [49]. To generate appropriate output, the input data set is supplied to the input layer, which is then processed by the hidden layers and output layer. A graphical representation of the multilayer perceptron model has been shown in Fig. 4.7.

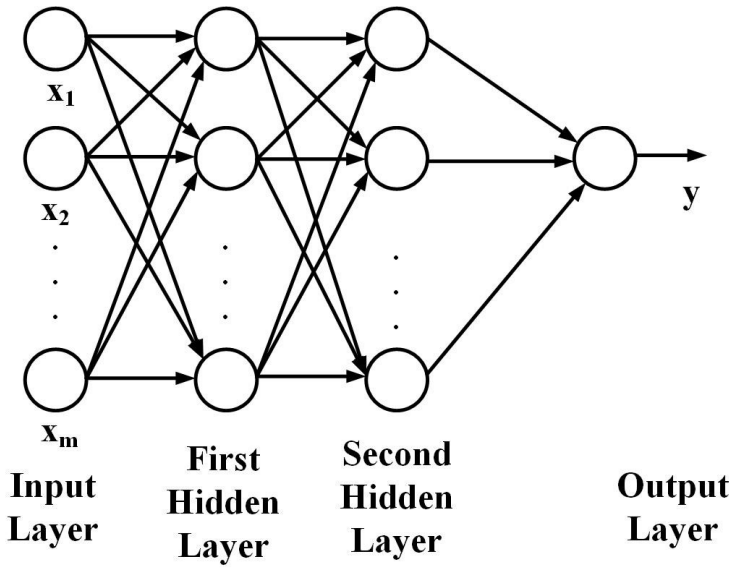


**Fig. 4.7 Multi-layer Perceptron Model**

The number of neurons in the input layer is determined by the number of input variables that have been used to forecast the output. Hidden layer neurons are chosen in such a way that system performance and complexity are balanced. The amount of output parameters to be controlled will determine the number of neurons in the output layer. In order to map the input pattern with the desired output, the network is trained based on the error in the actual output and the desired output. The weights of synaptic connections connecting different levels are adjusted to accomplish this.

### 4.3.4 Types of Learning

There are two forms of ANN-based machine learning: supervised learning and unsupervised learning [51]. The supervised learning is similar to learning by instruction in that the ANN is trained using a large number of training sets. To generate a functional mapping between the inputs and outputs, the training set takes the system's input characteristics and the output data that has been determined earlier by some experimental means or human judgments. The performance of the neural network model is checked and monitored during the training phase. This function compares the anticipated NN output to the actual output. The ANN continues to train each iteration until the error value is reduced to the target value. The ANN is then assessed using new data when the training is complete to determine its responsiveness and quality.

The network is enhanced using the unsupervised learning technique based on the nature of the inputs and the relationship between the inputs and outputs without the knowledge of the target output values. The notion is that comparable data tend to produce similar types of output. And, in many cases, unsupervised procedures are simply the first step of a two- or three-stage training process, with following phases using supervised learning. For example, the first training stage utilizes an unsupervised technique to identify the positions and sizes of the fundamental functions.

### 4.3.5 Control Scheme of ANN based MPPT of PV Array

The ratio of change in P and change in V is employed as error (e) in the ANN based control method, and change in error (e) is evaluated by subtracting error at the instant prior to the present from the error at the present instant of time, as illustrated in (4.21) and (4.22) similar to FLC:

$$e(k) = \frac{\Delta P(k)}{\Delta V(k)} \tag{4.21}$$

$$\Delta e(k) = e(k) - e(k-1) \tag{4.22}$$

The controller used in this work requires two inputs and thus utilizes two input neurons. For simplicity, only one hidden layer has been used which consists of 10 neurons by default. The output is the incremental change in duty cycle, thus there will be only one output neuron in the output layer of the controller. The synaptic weights are accordingly adjusted during the duration of the training based on the given desirable dataset. Thus, the learning used in the designed controller is a type of supervised learning.

## 4.4 ADAPTIVE NEURO-FUZZY INFERENCE SYSTEMS (ANFIS) BASED CONTROL

A neuro-fuzzy inference system (ANFIS) combines the two approaches previously mentioned, namely fuzzy logic and ANN-based controllers. Due to its increased adaptivity to manage dynamic and non-linear fluctuations in input circumstances, this combination of the two produces a superior response [52]. The block diagram of ANFIS, which combines the FLC and ANN modules, is shown in Fig.4.8 [34]. The Sugeno fuzzy model is the most frequently used of several FIS models.

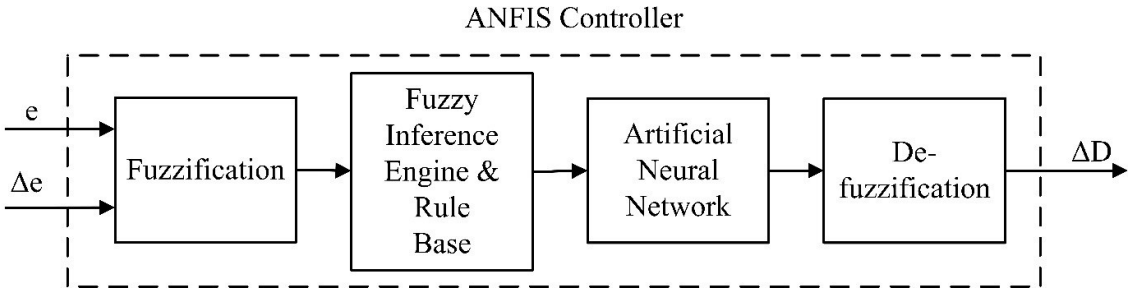


**Fig. 4.8 Basic block diagram of the ANFIS based controller**

It is a data-driven method for solving function approximation issues using a neural network approach. The majority of data-driven ANFIS network synthesis techniques are based on clustering a training set of numerical samples of the unknown function to be approximated. ANFIS networks have been effectively used to classification tasks, rule-based process control, pattern recognition, and other challenges since their inception.

### 4.4.1 Evolution of ANFIS

Jang [53] was the first to introduce the Adaptive Neuro-Fuzzy Inference System (ANFIS). ANFIS is a neural network that functions similarly to a Takagi Sugeno type inference model however, it is a hybrid intelligent system that combines ANN and fuzzy logic principles in one system. The ANFIS is given the capacity to learn from training data by using the ANN method to update the parameters of the Takagi Sugeno type inference model. As a result, the answers mapped out on a Fuzzy Inference System (FIS) may be expressed linguistically.

### 4.4.2 Basic Structure of ANFIS

Five separate layers are utilized to describe the structure of an ANFIS classifier in order to illustrate the idea of ANFIS structure. The fuzzification layer is the first layer in the ANFIS structure; the rule base layer is the second layer; the normalization of membership functions

(MFs) is the third layer; and the defuzzification and summation layers are the fourth and fifth layers, respectively as shown in Fig. 4.9.

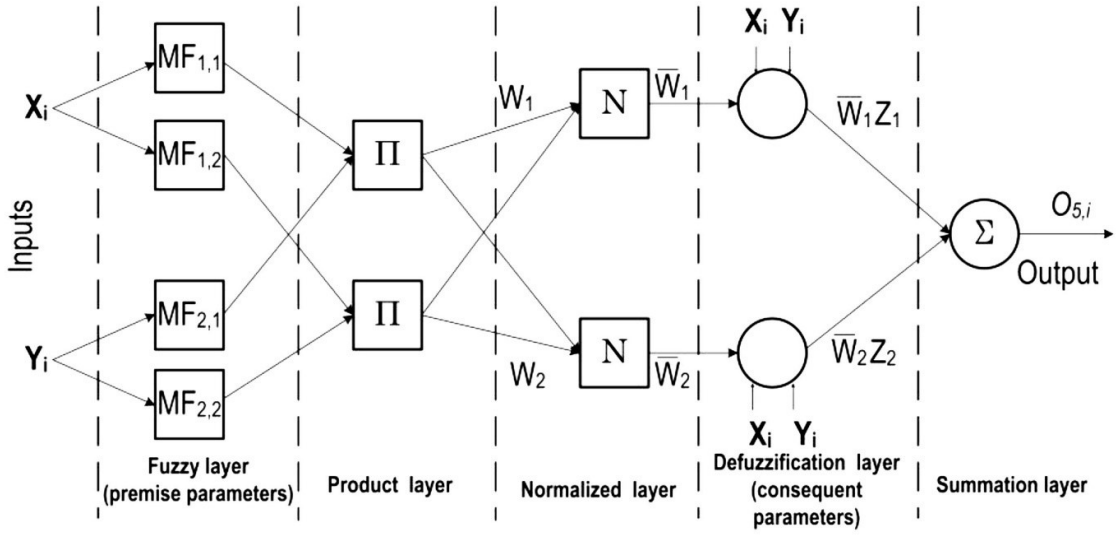


**Fig. 4.9 Basic Structure of the ANFIS based controller**

### 4.4.3 Design of an ANFIS based Controller

The design of an ANFIS classifier is divided into two parts: development and training. Selecting input variables, input space partitioning, picking the number/type of MFs for inputs, creating fuzzy rules, premise and conclusion sections of fuzzy rules, and selecting starting parameters for MFs are all part of the development process. To develop an ANFIS classifier, you must first produce training data patterns. ANFIS classifier inputs and the intended output make up these data patterns. However, when data production is an expensive endeavor, the size of the input-output data pattern is critical.

### 4.4.4 Learning Algorithms for ANFIS

The input-output data must be divided into rule patches before the ANFIS classifier can be built. Grid partitioning, subtractive clustering, and fuzzy c means (FCM) are some of the

approaches that may be used [54]. Grid partition is only effective for applications with a small number of input variables [53]. Traditionally, ANFIS classifiers have been restricted to low-dimensional modelling. It's worth noting that a good input partition can reduce the number of rules and therefore improve performance in both the learning and application stages. A learning method is used to modify the synaptic weights of the neurons in order to maximize the classifier's performance. The membership function settings in the training section can be changed throughout the learning process. The supervised learning of the input-output dataset that is supplied to the classifier as training data aids in the modification of these parameters. To tackle this training problem, many learning approaches may be employed, such as a hybrid-learning algorithm combining the least squares method with the gradient descent method.

### 4.4.5 Control Scheme of ANFIS based MPPT of PV Array

The ratio of change in P and change in V is employed as error (e) in the ANFIS based control method, and change in error (e) is evaluated by subtracting error at the instant prior to the present from the error at the present instant of time, as illustrated in (4.23) and (4.24) similar to FLC as well as ANN as discussed earlier.

$$e(k) = \frac{\Delta P(k)}{\Delta V(k)} \tag{4.23}$$

$$\Delta e(k) = e(k) - e(k-1) \tag{4.24}$$

The hybrid optimization approach was used to design the FIS, which was done through grid partitioning [55]. Unlike fuzzy systems, which require manual rule addition, the ANFIS controller adjusts its rules to the dataset. The inclusion of the ANN within the ANFIS controller is responsible for this intrinsic prediction capacity. The ANFIS controller is designed using a Takagi-Sugeno fuzzy inference system (FIS) based on the test dataset.

Seven generalized bell membership functions for the inputs as well output were used in this study as these membership functions are better at dealing with non-linear distributions. The discussed membership functions have been depicted in Fig. 4.10.

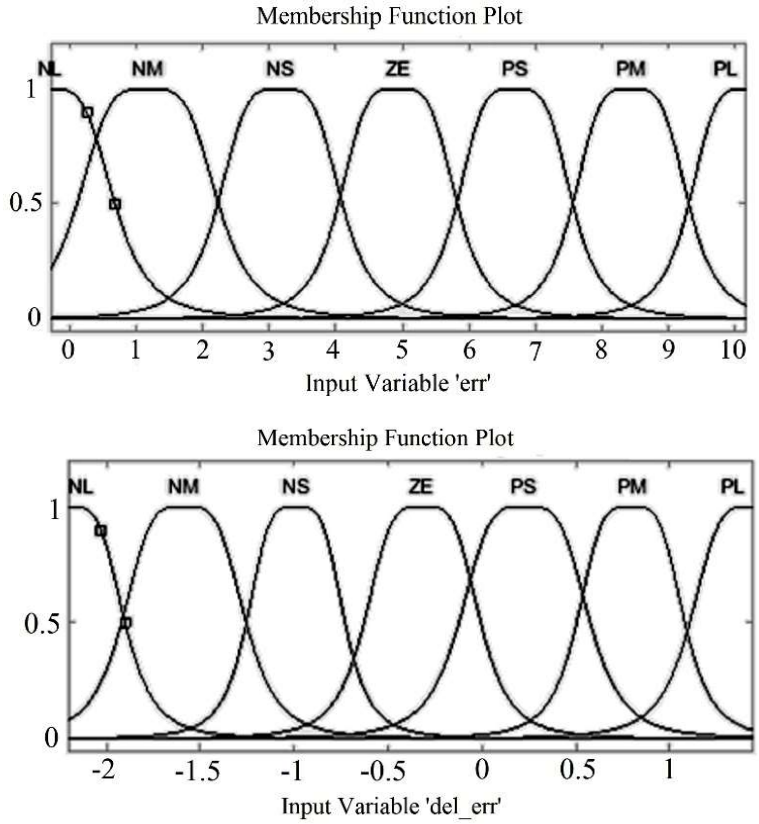


**Fig. 4.10 Membership functions for input variables of ANFIS based controller**

## 4.5 SIMULATION RESULTS & COMPARATIVE ANALYSIS

The plots obtained for power, voltage, current and duty ratio for the conventional as well as AI based controllers have been depicted in Fig. 4.11. The GMPPs for the irradiation sets in the format [$Irr_1$; $Irr_2$; $Irr_3$] used in Simulink have been tabulated in Table 4.2. The computation times for the five controllers i.e., P&O, InC, fuzzy logic, ANN and ANFIS based controllers have been tabulated in Table 4.3. It is observed that the ANN based

controller takes the least computation time i.e. approximately 3.31 minutes for a simulation of 2 s.

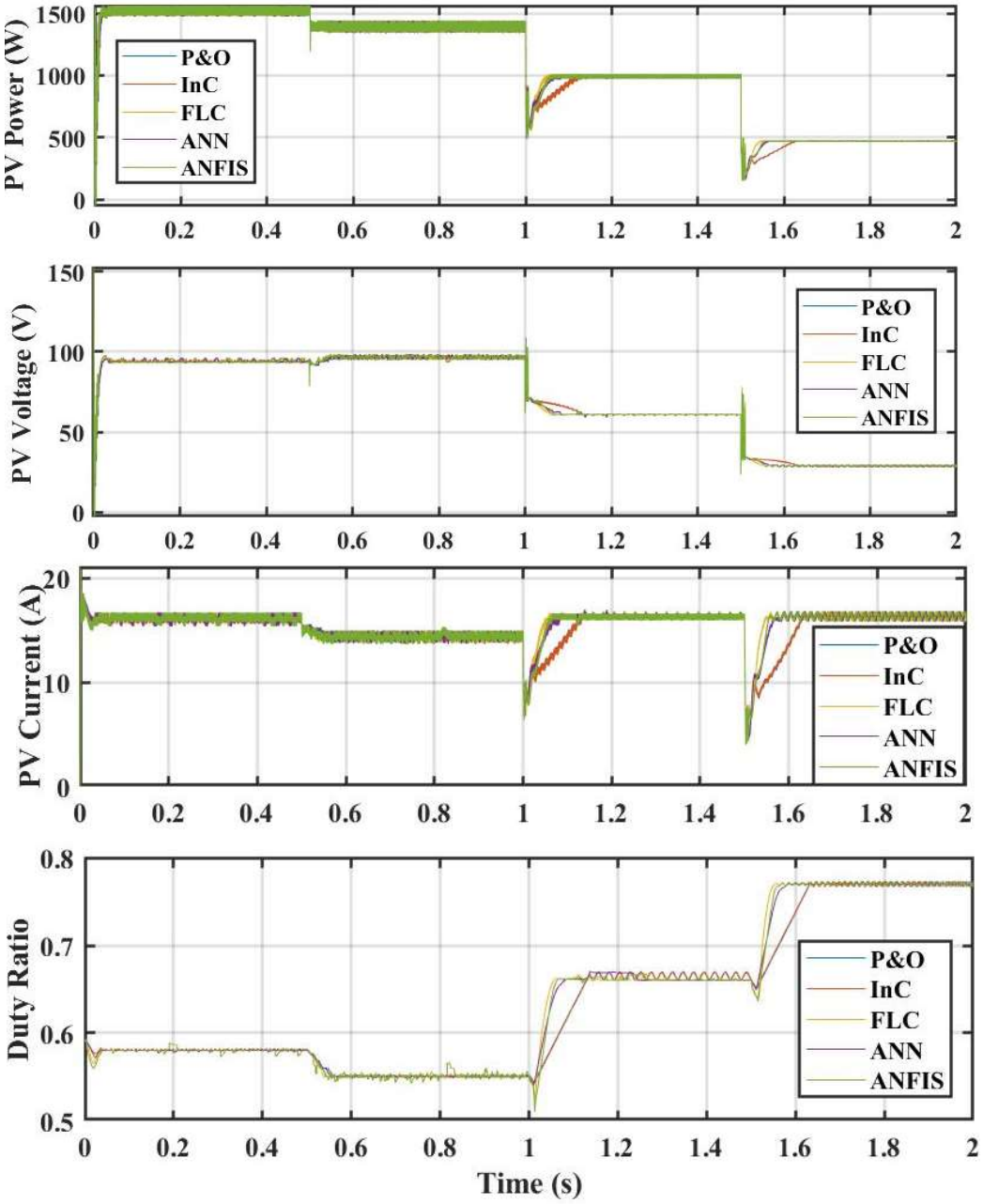


**Fig. 4.11 Comparative plots for PV power, voltage, current and duty ratio w.r.t. time for the discussed controllers.**

**Table 4.2 GMPP for the irradiation test sets**

| Irradiation Test Set (W/m$^2$) | GMPP (W) |
|---|---|
| [1000; 1000; 1000] | 1500 |
| [900; 900; 1000] | 1382 |
| [1000; 400; 1000] | 986.29 |
| [1000; 250; 250] | 469.4346 |
| [1000; 200; 200] | 469.4004 |

From Table 4.2, it can inferred that for a shading pattern with uniform irradiance of 1000 W/m$^2$, the GMPP would be 1500 W. Similarly, for [900; 900; 1000] i.e., $Irr_1$= 900 W/ m$^2$, $Irr_2$= 900 W/m$^2$, and $Irr_3$= 1000 W/m$^2$, the GMPP will lie at a value of 1382 W. For the patterns, [1000; 400; 1000], [1000; 250; 250] and [1000; 200; 200], the GMPPs will lie at a power of 986.29 W, 469.4346 and 469.4004 W respectively.

**Table 4.3 Comparative analysis of Computational Times of Conventional & AI based controllers**

| Control Technique | Computation Time (s) |
|---|---|
| **P&O** | 726.57 |
| **InC** | 241.21 |
| **FLC** | 1669.27 |
| **ANN** | 198.89 |
| **ANFIS** | 2160.69 |

Parameters like tracked power, settling time and tracking efficiency for the controllers have been compared in Table 4.4. It is observed that all the controllers have an efficiency of the order of 98 to 99%. However, FLC takes the least settling time in all the 4 test cases i.e. 0.026 s, 0.001 s, 0.056 s and 0.047 s, respectively. However, the ANN based controller has the

highest tracking efficiency of 99.27%, 99.93% and 99.44% in the second, third and fourth test case.

**Table 4.4 Comparative analysis of Tracking Parameters of Conventional & AI based controllers.**

| | Control Technique | Power Tracked (W) | Settling Time (s) | Tracking Efficiency (%) |
|---|---|---|---|---|
| **Test Case-1** | **P&O** | 1519 | 0.032 | 98.73 |
| | **InC** | 1521 | 0.034 | 98.6 |
| | **FLC** | 1522 | 0.026 | 98.53 |
| | **ANN** | 1521 | 0.0202 | 98.6 |
| | **ANFIS** | 1525 | 0.0292 | 98.34 |
| **Test Case-2** | **P&O** | 1398 | 0.022 | 98.69 |
| | **InC** | 1395 | 0.0203 | 98.91 |
| | **FLC** | 1394 | 0.001 | 98.98 |
| | **ANN** | 1390 | 0.0024 | 99.27 |
| | **ANFIS** | 1393 | 0.0014 | 99.05 |
| **Test Case-3** | **P&O** | 997.4 | 0.131 | 98.92 |
| | **InC** | 997.7 | 0.131 | 98.89 |
| | **FLC** | 997.1 | 0.056 | 98.95 |
| | **ANN** | 987.4 | 0.064 | 99.93 |
| | **ANFIS** | 989.1 | 0.057 | 99.76 |
| **Test Case-4** | **P&O** | 475.3 | 0.132 | 98.96 |
| | **InC** | 474.3 | 0.127 | 99.17 |
| | **FLC** | 473.7 | 0.047 | 99.3 |
| | **ANN** | 473 | 0.056 | 99.44 |
| | **ANFIS** | 473 | 0.053 | 99.44 |

## 4.6 CONCLUSIONS

It is observed that though the conventional algorithms are at par with the AI based technique in terms of power tracking, the AI based techniques have an edge over them, when it comes to the settling time. The AI based controllers settle in a relatively lesser time. Among the AI based controllers, FLC takes the least settling time and ANFIS shows an intermediate performance

compared to FLC and ANN. However, large computational time is taken by FLC and ANFIS and thus, ANN based controller seems to be a suitable contender.

# Chapter 5

# ANN based Learning Algorithms

A learning algorithm is the technique utilized for the learning process in an ANN. The learning algorithms entail a systematic change of the network's synaptic weights in order to attain a certain goal. Levenberg Marquardt (LM), Bayesian Regularization (BR), and Scaled Conjugate Gradient (SCG) are the three methods discussed in this work, and they are all meant to measure PV output under partial shading situations. Under variable irradiance and shade circumstances, the performance of these three learning algorithms is thoroughly examined. The error back propagation technique is used in all of the algorithms, in which the difference between the actual and intended output is transmitted backward to update the weights of the layers in a multilayer neural network.

## 5.1 LEVENBERG MARQUARDT (LM) ALGORITHM

A frequently used learning algorithm is the Levenberg Marquardt technique. It is a combination of the two approaches, namely the Newton's method and the Gradient Descent Method. When using Newton's technique, there is a quick convergence around the local or global minima, but if the method is poorly developed, there may also be a divergence. The Gradient Descent Method, on the other hand, ensures convergence, though it may be slower depending on the ideal step-size value used.

In a second-order function F(w), the ideal weight adjustment that has to be performed to parameter vector w is given by (5.1).

$$\Delta w = [H + \lambda I]g \tag{5.1}$$

where I is the identity matrix and λ is the regularizing parameter, g, the gradient vector and H, the Hessian matrix. The regularizing parameter is a significant variable as when it approaches zero, the LM algorithm begins to behave like Newton's technique; but, as it approaches a higher number, it begins to behave like the Gradient Descent Method of training. As a result, the weight is changed to $w_{k+1}$.

Without calculating the Hessian matrix, the LM method is utilized to achieve second-order training speed. The Hessian matrix H can be estimated as (5.2) in the terms of Jacobian matrix J, for a performance function in the format of sum of squares.

$$H = J^T J \tag{5.2}$$

The gradient vector can be substituted as (5.3).

$$g = J^T e \tag{5.3}$$

The error vector e is a matrix containing the difference between the desired and the actual outputs where $y_i$ represents the actual output of the controller while $d_i$ represents the desired output of the controller.

$$e = \frac{1}{2}\sum_{i=1}^{n}(d_i - y_i) \tag{5.4}$$

The modified weight $w_{k+1}$ can thus be written as (5.5).

$$w_{k+1} = w_k - \Delta w \tag{5.5}$$

The value of the regularizing parameter should be tweaked. If the performance function advances toward optimization, its value decreases after each step; otherwise, it increases.

## 5.2 BAYESIAN REGULARIZATION (BR) ALGORITHM

The input weights and bias values are adjusted in Bayesian Regularization in a similar manner as the LM optimization. In order to obtain greater generalization, BR not only minimizes the squared error, but also the network weights. Based on this, the training objective function is developed in (5.6).

$$F(w) = \alpha E_w + \beta E_D \tag{5.6}$$

The entire sum of squares of the weights in a network is $E_w$, the sum of network errors is $E_D$, and the objective function parameters are α and β. Based on Bayes' theorem [56], the values of the objective functions are computed. The network weights are assumed to be random variables in BR, and the weight distribution is assumed to be Gaussian.

The output of the controller is computed using the activations and synaptic weight estimates for the ANN to be developed as shown in (5.7).

$$\hat{y} = b^{k+1} + \sum_{j=1}^{m} w_j^{k+1} h_i^k \tag{5.7}$$

For the optimization purpose, the mean square error i.e., the MSE between the desired and obtained output values serves as the cost function. This cost function can be expressed as (5.8).

$$E = \frac{1}{n}\sum_{i=1}^{n}(y_i - \hat{y}_i)^2 \tag{5.8}$$

To avoid the problem of over-fitting as well as under-fitting, regularization is done. A parameter γ, known as the regularizing parameter is introduced such that it imposes a penalty on the MSE in case of over-fitting and under-fitting to the given dataset. This regularised error can be computed as (5.9).

$$E_R = \gamma E_w + (1 - \gamma) E_D \tag{5.9}$$

## 5.3 SCALED CONJUGATE GRADIENT (SCG) ALGORITHM

The search direction is an additional factor in the case of Scaled Conjugate Gradient method as compared to the previously discussed algorithms. A reduction in error is desirable such that the selected search direction helps the controller proceed towards convergence. Thus, a change in the synaptic weight based on the prevalent search direction is introduced as shown in eqn. (5.10).

$$\vec{w}_{k+1} = \vec{w}_k + \alpha_k \vec{p}_k \tag{5.10}$$

However, if no considerable reduction in error is observed, the search direction is updated using (5.11).

$$p_{k+1} = -g_{k+1} + \beta_k p_k \tag{5.11}$$

where g is the gradient of error which, if zero, implies that the desirable extrema has been reached. β can be written in the terms of gradient as (5.12).

$$\beta_k = \frac{(|g_{k+1}|^2 - g_{k+1}{}^T g_k)}{g_k{}^T g_k} \tag{5.12}$$

Thus, the modified search direction can be expressed in the terms of gradient of error as (5.13).

$$p_{k+1} = -g_{k+1} + \left(\frac{(|g_{k+1}|^2 - g_{k+1}{}^T g_k)}{g_k{}^T g_k}\right) p_k \tag{5.13}$$

## 5.4 BASIC ANN BASED CONTROLLER DESIGN WITH LEARNING ALGORITHM

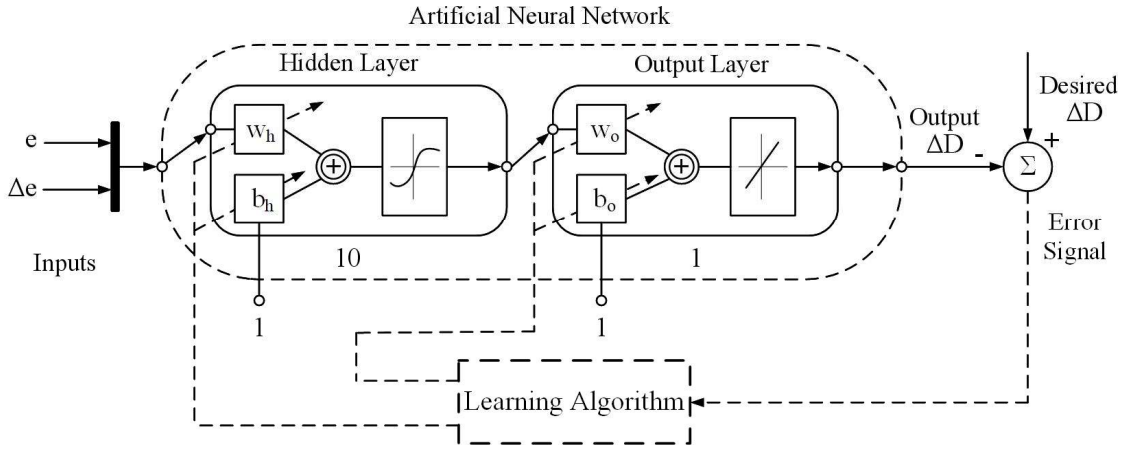


**Fig. 5.1 Block diagram of ANN based controller**

The designed controllers have two inputs, a hidden layer with ten hidden neurons and an output layer as illustrated in Fig. 3. The inputs to the controllers are error, denoted by e, and change in error, denoted by Δe as described in (4.21) and (4.22).

The controller generates the incremental change in duty cycle (ΔD) as the output. This incremental change modifies the present duty cycle ratio and with the help of a PWM

generator, generates the switching signals for the boost converter switch. The generated value of output ΔD is compared with the desired value of ΔD, which is included in the dataset, and an error signal is generated. The error signal acts as the input for the learning algorithm which modifies the synaptic weights and biases of the hidden layer and output layer. The initial input for the bias is taken as 1. Thus, learning algorithm plays a significant role in determining the response of a controller.

## 5.5 COMPARATIVE SIMULATION RESULTS & ANALYSIS

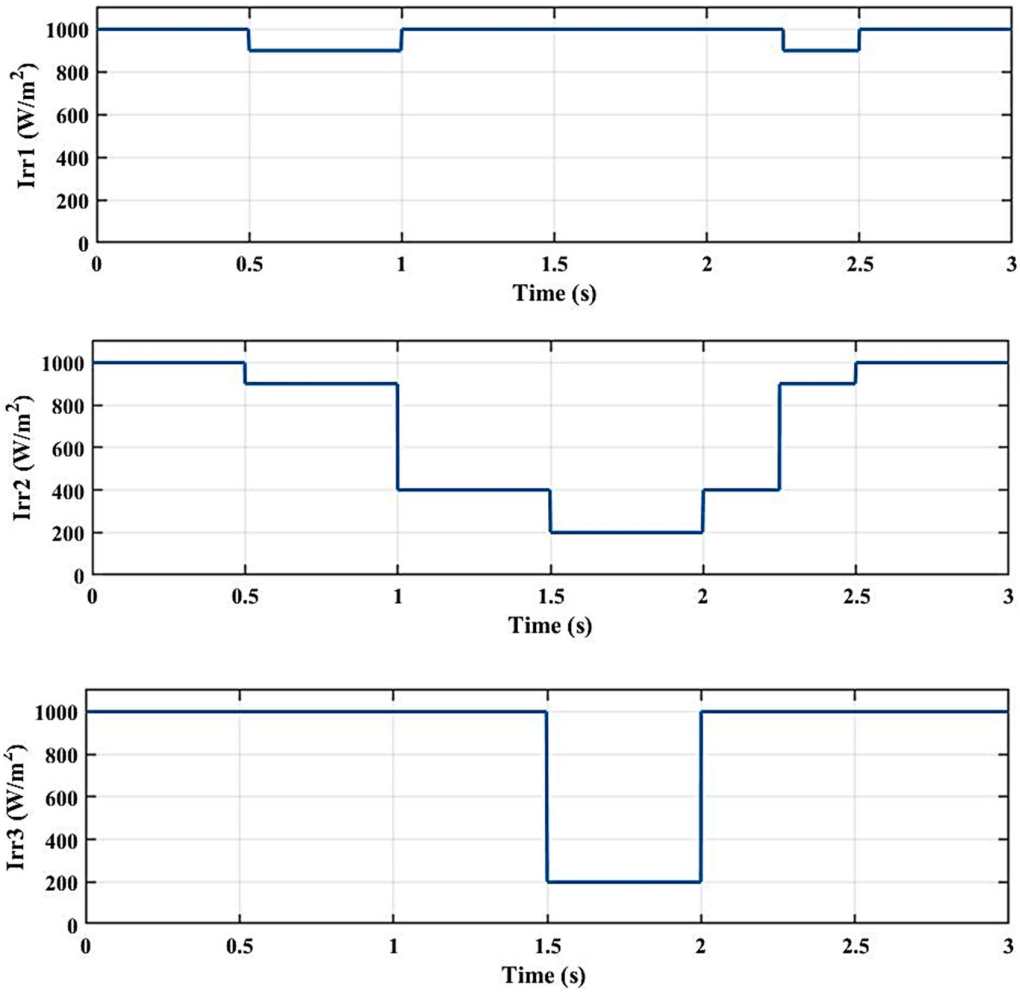


**Fig. 5.2 Variation of Irradiance in the test cases**

For an irradiance pattern as shown in Fig. 5.2, the designed controllers are tested. Further, a comparison is drawn between their testing as well as training performance. The shading at different locations of the array leads to the presence of multiple peaks of power known as local MPPs and the global peak is termed as the global MPP. An illustration of the occurrence of local and global MPPs is evident from the obtained P-V and I-V characteristics as shown in Fig. 5 (a) and (b) respectively.

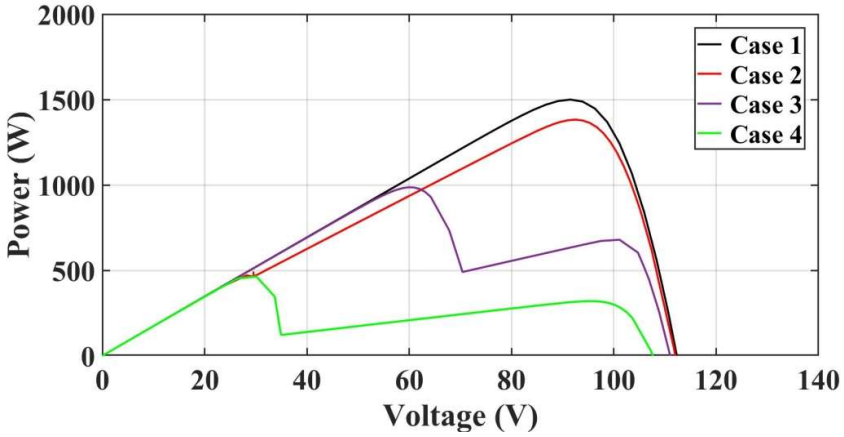


**(a)**

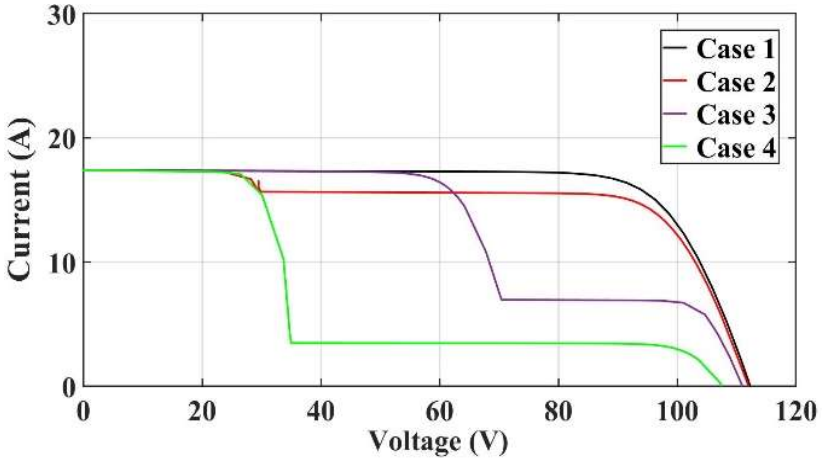


**(b)**

**Fig. 5.3 (a) P-V and (b) I-V characteristics of the PV array under the four test cases**

Under the four testing conditions, analysis is performed in terms of power, voltage, current and duty cycle as represented in Fig. 5.4 (a). The performance of all the designed controllers is quite similar in achieving the steady state conditions. However, to observe transient analysis closely an enlarged view during transient conditions is presented in Fig. 5.4 (b). This section also discusses the transient performance of LM algorithm vs. BR and SCG algorithms. Fig. 5.4 (b) depicts the dynamic response of the compared learning algorithms in the form of a zoomed version of the Fig. 5.4 (a). From Fig. 5.4 (b), it can be seen that LM algorithm reaches the MPP at a faster rate compared to the BR and SCG algorithms in most of the cases. However, SCG leads the LM based algorithm between 0.5 s and 1 s.

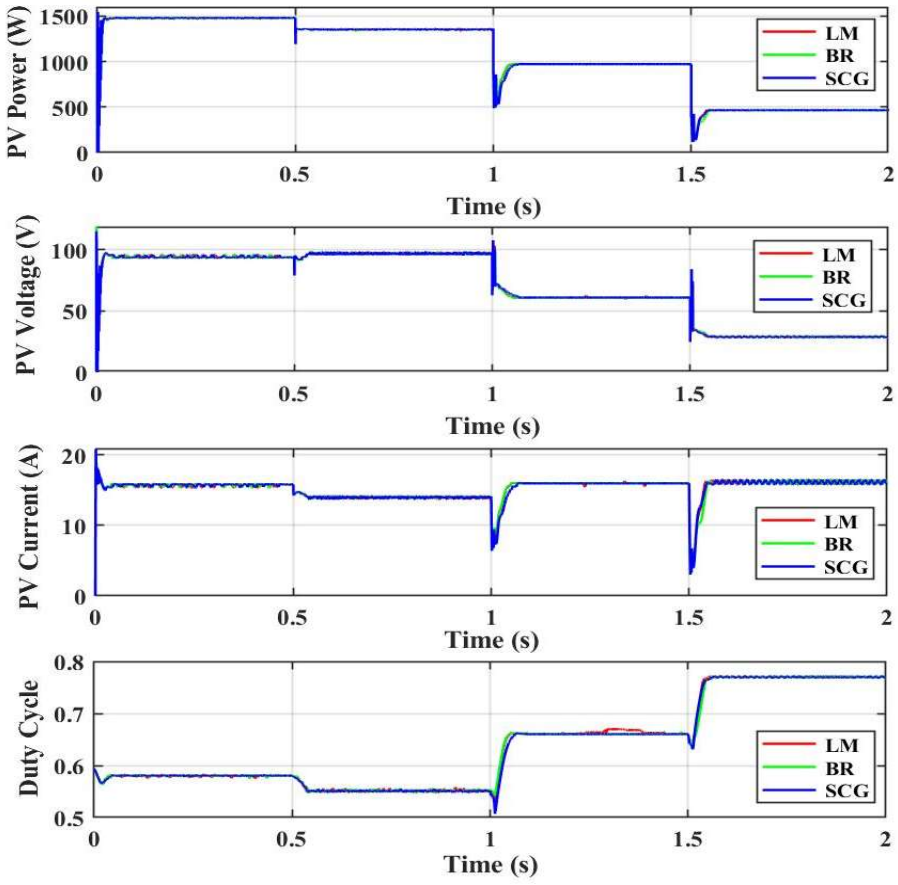


**Fig. 5.4 (a)Waveforms for PV output power, voltage, current and duty cycle for the test cases**

A comparative analysis of the performance of the three training algorithms is tabulated in Table 5.1 in terms of shading and mismatch losses occurring in the system, the fill factor as well as tracking efficiency for all the test cases. From Table 5.1, it is observed that though all the three control algorithms are properly designed and are highly efficient with a tracking efficiency of the order 98 to 99% and even higher. The Levenberg Marquardt algorithm-based controller gives the best performance under all the four test cases with an efficiency of 98.67%, 99.2 %, 99.21% and 99.44% in the first, second, third and fourth test case respectively.

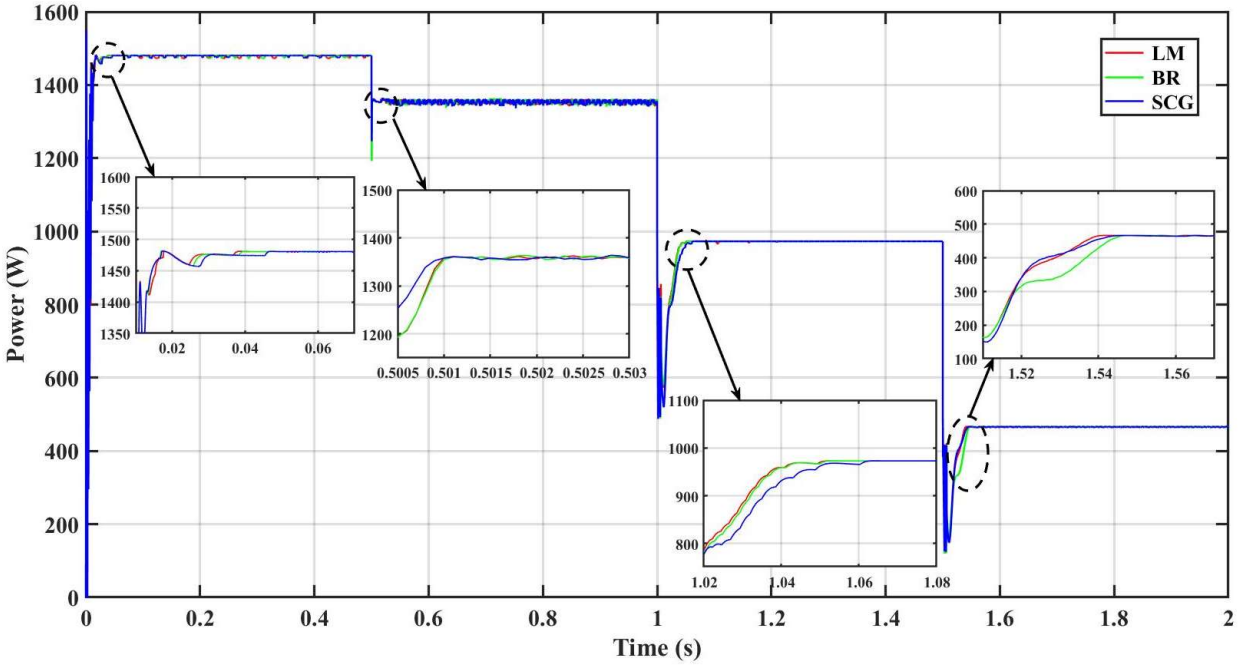


**Fig. 5.4 (b) Waveform for PV output power for the test cases**

**Table 5.1 Analysis of Tracking & Performance Parameters of a PV Array**

| Cases | Learning Algorithm | Shading Losses(W) | Shading Losses (%) | Mismatch Losses(W) | Mismatch Losses (%) | Fill Factor | Tracking Efficiency (%) |
|---|---|---|---|---|---|---|---|
| Case-1 | LM | 20 | 1.34 | 19.3 | 1.28 | 0.753 | 98.67 |
| | BR | 22 | 1.47 | 21.3 | 1.42 | 0.752 | 98.53 |
| | SCG | 22 | 1.47 | 21.3 | 1.42 | 0.752 | 98.53 |
| Case-2 | LM | 129 | 8.6 | 46.8 | 3.3 | 0.697 | 99.2 |
| | BR | 131 | 8.74 | 48.8 | 3.44 | 0.696 | 99.05 |
| | SCG | 132 | 8.8 | 49.8 | 3.51 | 0.695 | 98.98 |
| Case-3 | LM | 521.42 | 34.76 | 221.02 | 18.43 | 0.498 | 99.21 |
| | BR | 521.42 | 34.76 | 221.02 | 18.43 | 0.498 | 99.21 |
| | SCG | 521.42 | 34.76 | 221.02 | 18.43 | 0.498 | 99.21 |
| Case-4 | LM | 1032.82 | 68.85 | 219.75 | 31.98 | 0.237 | 99.44 |
| | BR | 1032.92 | 68.86 | 219.85 | 32 | 0.238 | 99.41 |
| | SCG | 1032.92 | 68.86 | 219.85 | 32 | 0.238 | 99.41 |

It is also observed that the performance of the three algorithms is quite comparable for the third and fourth test case i.e., as the irradiation level decreases, the difference between the performances of the three controllers drops considerably. LM algorithm-based controller has the least amount of shading and mismatch losses as can be observed from Table 5.1. The fill factor is an important factor to determine the efficiency of a PV array. The closer the value of fill factor approaches to 1, the better is the efficiency of the array. In Table 5.1, the fill factor drops considerably as the irradiance decreases from the first test case to the fourth test case.

## Training Performance

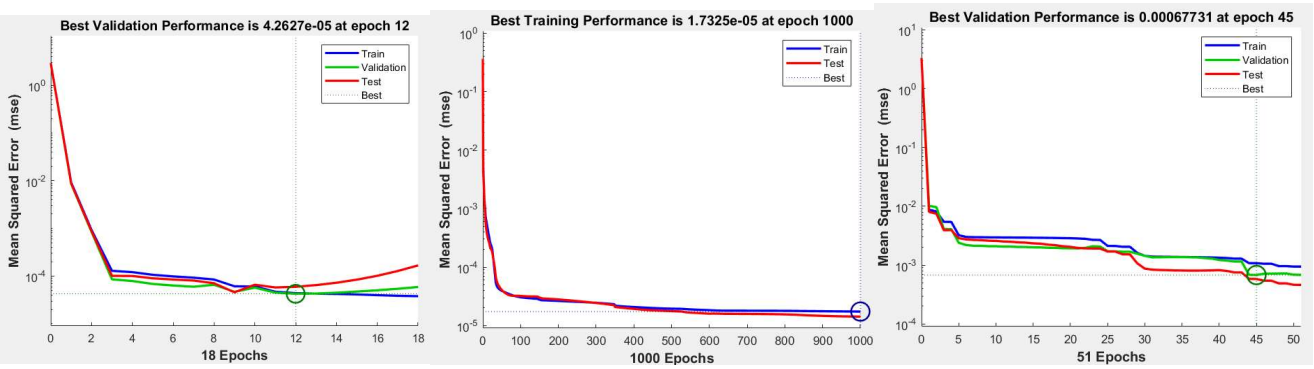


**Fig. 5.5 MSE vs. Epoch plot for (a) LM, (b) BR and (c) SCG algorithms**

Table 5.2 includes the comparative analysis of training parameters. MSE plays an essential role in determining the variation in the obtained output from the target values. A smaller value of MSE is desirable. Regression R values are a measure of the correlation between the obtained output values and the target values. It is known that the value of R close to 1 shows a close relationship among the quantities. A zero value of R indicates a random relationship. From Table 5.2, it can be concluded that BR has the least testing MSE of $1.42\times10^{-5}$, followed by SCG and LM having a MSE of $5.7988\times10^{-5}$ and $5.975\times10^{-5}$ respectively. The R values for testing, in the Table indicate that the output and target share a closer relationship in the case of BR based ANN controller with R value of 0.999 and quite similar is the case of LM and SCG with R value of 0.998 and 0.971 respectively.

**Table 5.2 Analysis of Training Performance Parameters of a PV Array**

| Learning Algorithm | MSE ($10^{-5}$) | | | R | | | Epoch | Training Time (s) | Performance (MSE) | Gradient |
|---|---|---|---|---|---|---|---|---|---|---|
| | Training | Validation | Testing | Training | Validation | Testing | | | | |
| LM | 4.397 | 4.263 | 5.975 | 0.998 | 0.997 | 0.998 | 18 | 9 | $3.8\times10^{-5}$ | 0.00214 |
| BR | 1.732 | 0 | 1.42 | 0.999 | 0 | 0.999 | 1000 | 25 | $1.73\times10^{-5}$ | $5.7\times10^{-5}$ |
| SCG | 1.076 | 6.773 | 5.7988 | 0.957 | 0.953 | 0.971 | 51 | 0 | $94.2\times10^{-5}$ | 0.00275 |

From Table 5.2, it is clearly evident that the LM based ANN technique takes lesser epochs for reaching convergence i.e., 18 epochs; however, it takes a larger time per iteration as compared to SCG where 51 epochs are completed in less than a second. The Mean Square Normalized Error Performance function for the three controllers has also been compared and it can be inferred from Table 5.2 that BR has the least value of the performance function i.e., $1.73\times10^{-5}$, followed by LM and SCG with a value of 3.8 × 10-5 and $94.2\times10^{-5}$ respectively. Gradient gives an idea about tuning the parameters in a way which leads to minimization of error. Gradient is inversely proportional to the learning rate and hence a smaller value of gradient indicates a larger learning rate. Thus, BR has the highest learning rate among the three for the given dataset, owing to the least value of gradient i.e., $5.7\times10^{-5}$, as can be observed from Table 5.2.

The MSE vs. Epoch plots for the three algorithms have been depicted in Fig. 5.5. From the plots, it can be seen that for LM, the best validation performance is $4.2627\times10^{-5}$ at epoch 12 for 18 epochs in all. While for BR algorithm, the best training performance is $1.7325\times10^{-5}$ at epoch 1000. For SCG, the best validation performance obtained is $67.731\times10^{-5}$ at epoch 45 for 51 epochs in all.

## 5.6 CONCLUSIONS

In this work, the performance of three training algorithms for ANN based controller are compared under different test cases of partial shading conditions of PV array. ANN controllers handled the non-linear operating environment arising due to partial shading with perfection. The performance is compared under randomly varying irradiance condition for power tracking, shading losses, mismatch losses, fill factor as well as tracking efficiency, and LM based algorithms is found outperforming the other two counterparts in most of the scenarios. The performance is also tested on control parameters, such as performance indices, rise time, settling time, peak overshoot/ undershoot etc. Here also, LM based algorithm is scoring high in most of the cases and at par with others in very few cases. Rigorous

simulation studies have confirmed the effectiveness of LM algorithm as the most potential training algorithm for maximum power point tracking under partial shading conditions.

# Chapter 6

# Simplified Optimised Fuzzy Logic Controller

## 6.1 INTRODUCTION

Due of their high adaptability to changes in operating circumstances and improved response to non-linearities, fuzzy logic-based controllers have received intriguing attention. The amount of time these controllers take for computation has however been a major problem [57-58]. By utilizing the proposed simplified as well as optimized version of fuzzy logic controller, this computational load might can be minimized. In this chapter, a simplified as well as optimized FLC (SOFLC) is presented, which comprises of a 4-rule base FLC along with a compensating polynomial, which reduces the FLC's structural complexity, computational burden and time.

## 6.2 PROPOSED CONTROLLER

In order to reduce the structural complexity of the designed controller, an FLC with least number of rules is designed. Since there are two inputs to the controller i.e., error and change in error, the least or minimum rules for the controller will be 4 i.e., 2×2. The rule base for a 4 rule FLC is tabulated in Table 6.1. The membership functions for the 4 rule FLC inputs and output have been shown in Fig. 6.1 and Fig. 6.2 respectively.

**Table 6.1 Rule Base for a 4-rule FLC**

| **e/ Δe** | **N** | **P** |
|---|---|---|
| **N** | P | ZE |
| **P** | ZE | N |

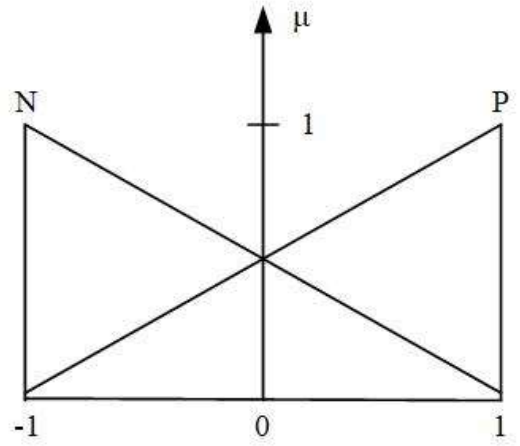


**Fig. 6.1 Triangular membership function for inputs of 4 rule FLC**

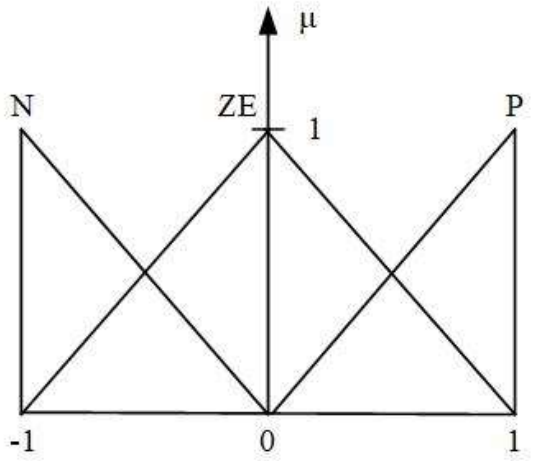


**Fig. 6.2 Triangular membership function for output of 4 rule FLC**

The strategy for the design of this least complex controller is such that the proposed controller should be able to produce a response equivalent to that of a 49-rule base controller. Thus, the response of the proposed controller is plotted against the response of the 49-rule base FLC as shown in Fig. 6.3.

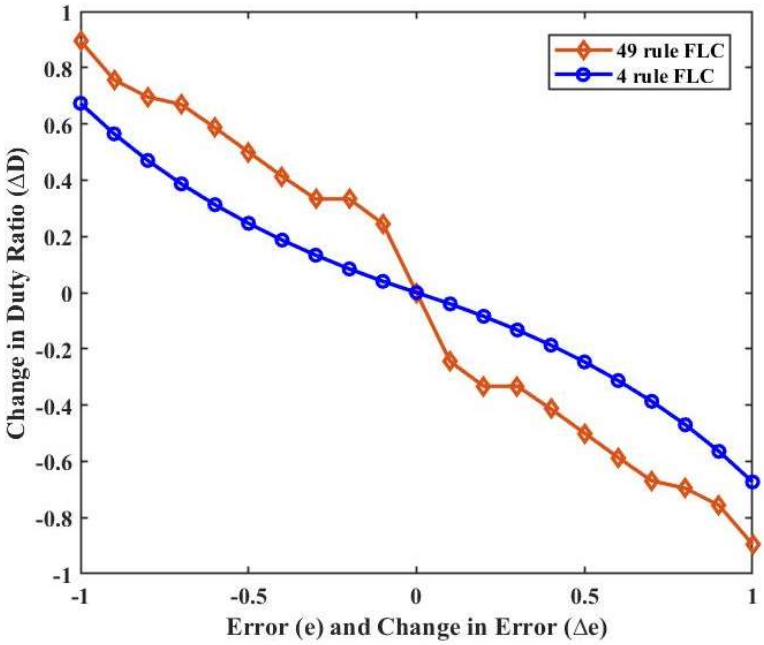


**Fig. 6.3 Response mapping of 49 and 4 rule FLC**

However, it is found that there is a wide gap between the two responses. To eliminate this difference between the two responses and to approximate the SOFLC with a performance equivalent to a 49-rule base FLC, a compensating polynomial is introduced as depicted in Fig. 6.4. This compensating polynomial can be evaluated using the polynomial fitting function.

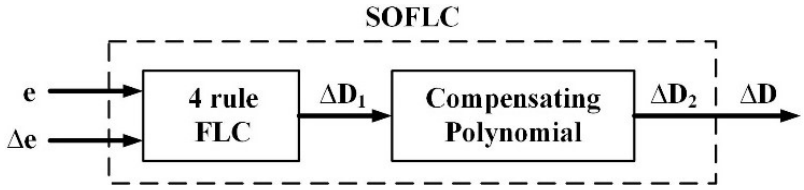


**Fig. 6.4 Proposed SOFLC**

The computed compensating polynomial is computed as (6.1).

$$\Delta D_2(t) = -34.5386\,\Delta {D_1}^7(t) + 36.1298\,\Delta {D_1}^5(t) - 12.6371\Delta {D_1}^3(t) + 2.8466\,\Delta D_1(t) \quad (6.1)$$

The MSE obtained for different orders of polynomials, as shown in Fig. 6.5, is used to pick the 7th order polynomial. Beyond order 7, the MSE is very low, therefore the 7th order polynomial gives the optimum balance between performance and complexity. The other error based performance parameters have been shown in Table 6.2.

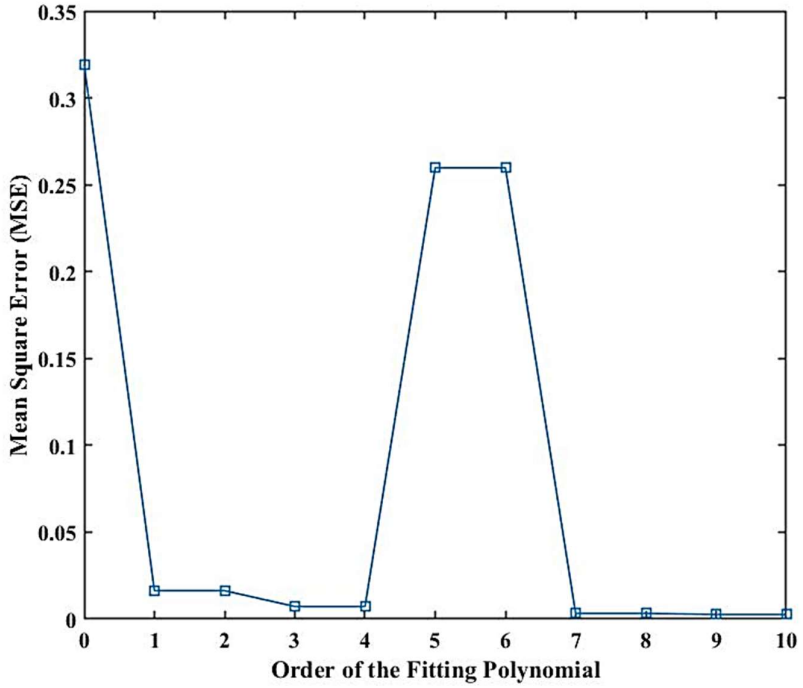


**Fig. 6.5 MSE vs Order of the Polynomial plot for the Compensating Polynomial**

**Table 6.2 Error based Performance Parameters**

| Order of the Polynomial | SSE | MSE | RMSE | S.D. | Variance | MAE | MPE (%) | MAPE (%) |
|---|---|---|---|---|---|---|---|---|
| **0** | 6.71 | 0.3193 | 0.565 | 0 | 0 | 0.517 | 117 | 117 |
| **1** | 0.343 | 0.0163 | 0.127 | 0.55 | 0.303 | 0.116 | 36.04 | 42.16 |
| **2** | 0.343 | 0.0163 | 0.127 | 0.55 | 0.303 | 0.116 | 36.04 | 42.16 |

| | | | | | | | | |
|---|---|---|---|---|---|---|---|---|
| **3** | 0.152 | 0.0072 | 0.085 | 0.559 | 0.312 | 0.067 | 29.87 | 34.69 |
| **4** | 0.152 | 0.0072 | 0.085 | 0.559 | 0.312 | 0.067 | 29.87 | 34.69 |
| **5** | 5.456 | 0.2598 | 0.509 | 1.029 | 1.059 | 0.351 | -15.07 | 74.19 |
| **6** | 5.456 | 0.2598 | 0.509 | 1.029 | 1.059 | 0.351 | -15.07 | 74.19 |
| **7** | **0.067** | **0.0032** | **0.056** | **0.562** | **0.316** | **0.04** | **28.29** | **33.9** |
| **8** | 0.067 | 0.0032 | 0.056 | 0.562 | 0.316 | 0.04 | 28.29 | 33.9 |
| **9** | 0.054 | 0.0026 | 0.051 | 0.563 | 0.317 | 0.04 | 29.29 | 33.9 |
| **10** | 0.054 | 0.0026 | 0.051 | 0.563 | 0.317 | 0.04 | 29.29 | 33.9 |

With the introduction of the compensating polynomial, the mapping of the SOFLC response is done w.r.t. the mapping of a 49 rule FLC as plotted in Fig. 6.6.

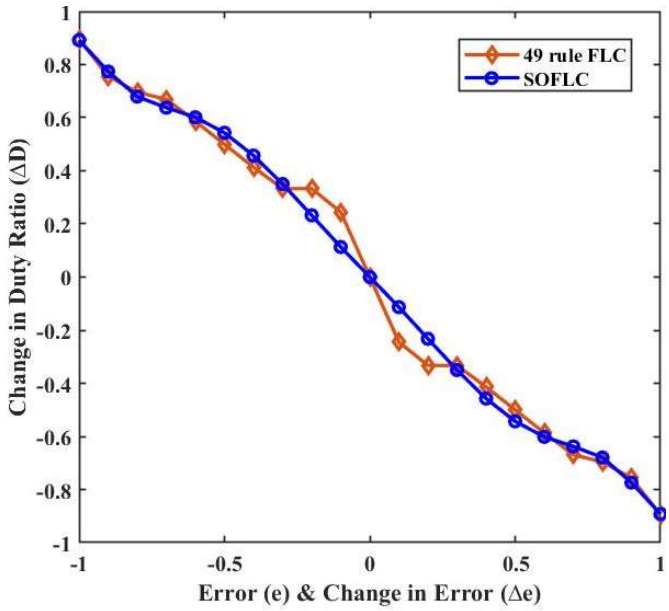


**Fig. 6.6 Response mapping of 49 and 4 rule SOFLC**

The output surface of the 49 as well as 4 rule FLC with respect to the inputs e and Δe has been plotted in Fig. 6.7 (a) and (b).

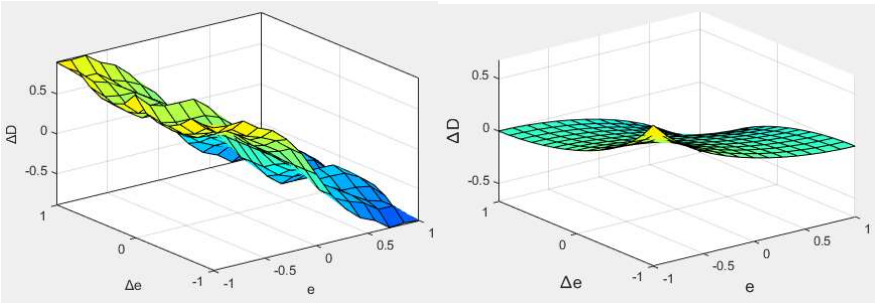


**Fig. 6.7 Output Surface of the (a) 49 rule and (b) 4 rule FLC**

## 6.3 SIMULATION RESULTS FOR THE PROPOSED CONTROLLER

The variation in Irr1, Irr2 and Irr3 has been shown in Fig. 6.8.

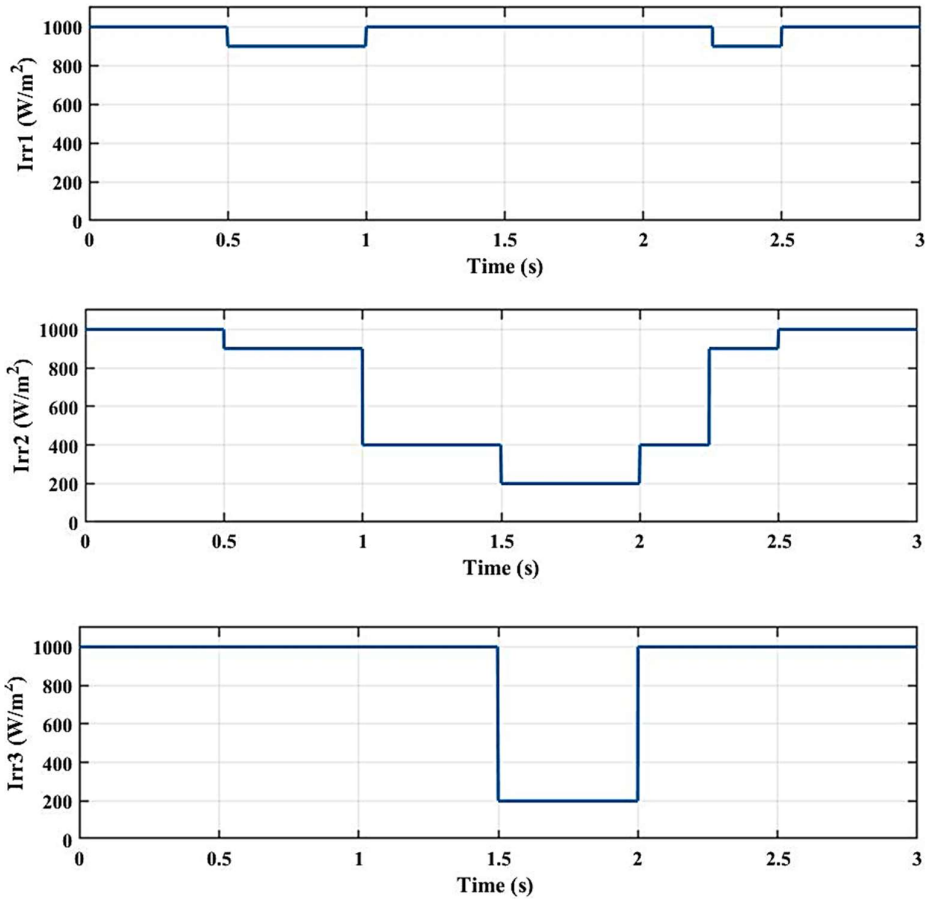


**Fig. 6.8 Variation of Irradiance in the four test cases.**

The P-V and I-V characteristics obtained for the above discussed test case have been illustrated in Fig. 3.8. The LMPPs and GMPPs have further been marked in Fig. 6.9.

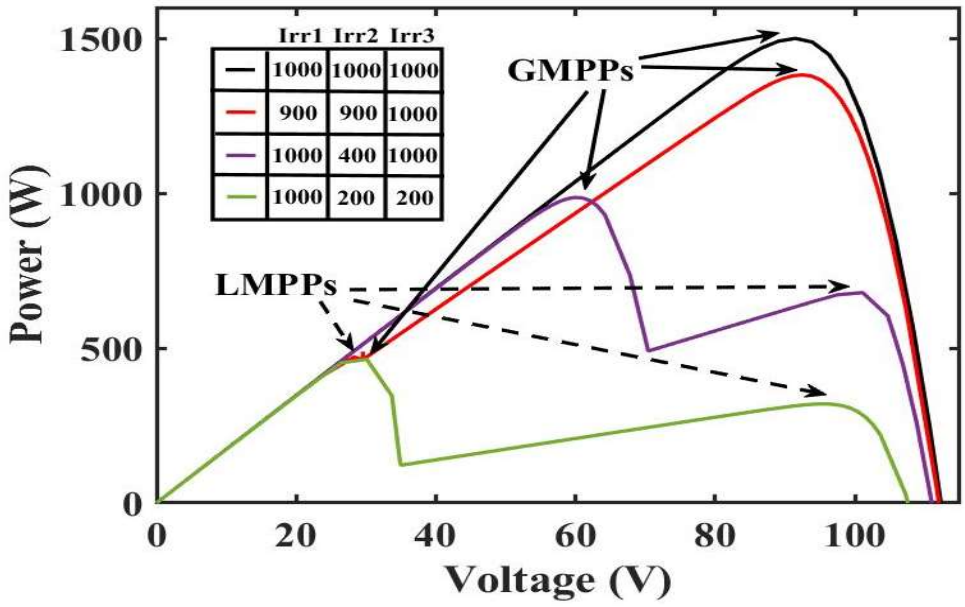


**Fig. 6.9 P-V & I-V characteristic of the designed array under the four test cases.**

The response plots for the proposed and conventional 49 rule FLC have been plotted in Fig. 6.10. They include the power output, the output voltage and current as well as the duty ratio of the controllers under comparison.

The MPP is being tracked by both the controllers i.e., the proposed 4 rule SOFLC and the 49 rule FLC. During MPPT, however, it can be seen that the SOFLC settles quicker than the 49-rule base FLC. Therefore, it can be inferred that SOFLC has a reduced rising time.

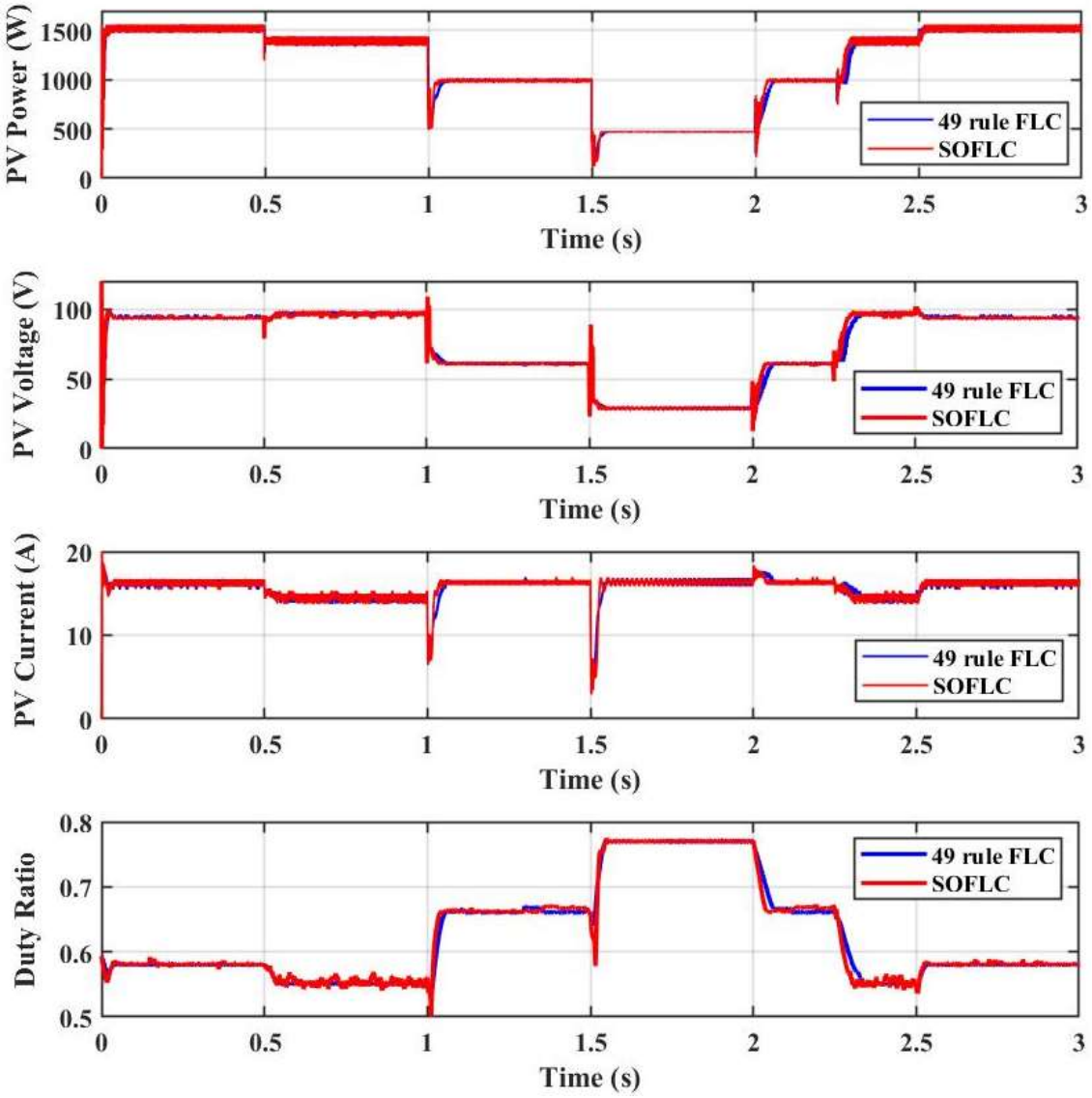


**Fig. 6.10 Response plots for the (a) 49 rule and (b) 4 rule SOFLC**

## 6.4 COMPARATIVE ANALYSIS

The comparative analysis of the proposed as well as conventional controller can be done in two ways i.e., the analysis based on the performance indices as well as the statistical analysis.

### 6.4.1 Analysis based on Performance Indices

A comparative analysis of the performance indices is presented in Table 6.2. A low value of these error based performance indices is desirable for an effective and efficient control system.

From Table 6.3, it can be observed that the 4 rule FLC has the highest value of the performance indices and thus is the most inefficient one among the controllers being compared here. The proposed SOFLC has the least range of these indices and thus appears to be the most suitable choice. The 49 rule base FLC has intermediate values of the indices; however the values approach towards the SOFLC as compared to the 4-rule FLC. Thus, the designed SOFLC shows slightly better performance w.r.t 49-rule FLC and much better as compared to 4-rule FLC.

**Table 6.3 Comparative Analysis of Performance Indices**

| Controller | IAE | ITAE | ISE ($10^4$) | ITSE ($10^4$) |
|---|---|---|---|---|
| **49-rule FLC** | 93.42 | 139.8 | 1.998 | 2.352 |
| **4-rule FLC** | 591.3 | 1323 | 30.15 | 70.49 |
| **SOFLC** | 86.04 | 123.9 | 1.831 | 1.945 |

### 6.4.2 Statistical Analysis of Controller Performance

A comparative statistical analysis of the 4-rule FLC and SOFLC has been tabulated in Table 6.4. It consists of the mean square error (MSE), standard deviation (S.D.), Variance, Mean Absolute Error (MAE) and Mean Percentage Error (MPE). These values are calculated with respect to the error between the response of the respective controllers and the 49-rule base FLC.

Mean square error (MSE) is the mean of the squared sum of errors. It is a measure of the closeness of the response obtained by the controller in comparison with the response obtained by the 49 rule FLC. From Table 6.4, it can be analysed that the SOFLC has a smaller MSE of

0.0032 and thus is a better approximated version of the 49-rule FLC as compared to its 4-rule counterpart.

The standard deviation (S.D.) and variance are indicative of the spread of the data around the mean value. The higher the value of S.D. and variance, the higher is the spread of the response around the mean value. Thus, SOFLC offers a wider range of control.

Mean absolute error (MAE) is a statistical tool for the calculation of the arithmetic mean of the absolute value of errors. SOFLC has a smaller value of MSE i.e., 0.04, which is desirable as compared to 4 rule FLC with a MAE of 0.222. Mean percentage error (MPE) is reduced in the case of SOFLC by a larger percentage of 17.46 % compared to the 4-rule FLC.

A plot of the absolute deviation with respect to error and change in error has been plotted in Fig. 6.11 to illustrate the large reduction in error due to the introduction of the compensating polynomial in the case of SOFLC.

**Table 6.4 Comparative Statistical Analysis**

| Controller | MSE | S.D. | Variance | MAE | MPE (%) |
|---|---|---|---|---|---|
| **4-rule FLC** | 0.0525 | 0.36 | 0.129 | 0.222 | 45.75 |
| **SOFLC** | 0.0032 | 0.56 | 0.316 | 0.04 | 28.29 |

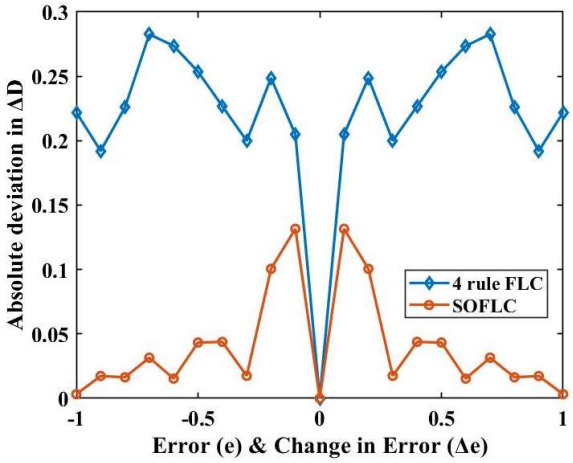


**Fig. 6.11 Plot of absolute deviation in PV Performance Parameters**

**Memory Requirement and Computational Efficiency**

The main stages of processing in a general FLC are fuzzification, fuzzy inference system (FIS) as well as knowledge base and de-fuzzification. The memory requirement for fuzzification and defuzzification modules is dependent on number of inputs and output variables, membership functions used for each variable and memory units required per membership function. For FIS and knowledge base module memory requirement is a function of number of rules, number of antecedents and consequents. However, in the case of SOFLC, due to the compensating polynomial, additional memory is required for processing apart from that of the general FLC. Due to the reduction in rules by a great extent, the memory requirement of a 4-rule FLC and proposed SOFLC with a compensating polynomial are quite less than the 49-rule FLC. However, the performance of proposed SOFLC is much better than 4-rule FLC and approximates a 49-rule FLC quite effectively.

A comparative analysis of memory requirement and computational time has been tabulated in Table 6.4. Memory requirement of the 49-rule base is $(21m_0+686)$ units, where $m_0$ is the memory requirement of each membership function. A 4-rule FLC takes the least memory i.e., $(7m_0+32)$ units but to have an improved performance and to approximate the 49-rule FLC action, the SOFLC is used which has a slightly more memory requirement i.e. $(7m_0+47)$ units. The computation time is a major issue in the case of FLCs. The simulations were performed on Intel(R) Core (TM) i5-1035G1 CPU with the processor base frequency of 1 GHz for a duration of 3 seconds under continuously varying irradiance. The SOFLC reduced the computation time of the 49-rule FLC by 2.5 times.

**Table 6.5 Comparative Analysis of Memory Requirement & Computational Time**

| Controller | Memory Requirement (units) | Ratio of Computational Time with respect to 49-rule FLC |
|---|---|---|
| **49 rule FLC** | $21m_0+686$ | 1:1 |
| **4-rule FLC** | $7m_0+32$ | 0.40:1 |
| **SOFLC** | $7m_0+47$ | 0.40:1 |

Thus, it is observed that the proposed SOFLC will be highly effective as compared to the conventional 49 rule FLC with a significant reduction in the computational burden as well as time.

## 6.5 CONCLUSIONS

Based on the analysis of the designed MPP techniques, Table 6.5 has tabulated. It is observed that the conventional MPP techniques offer a high tracking efficiency but take a higher computational as well as settling time compared to their AI counterparts. The least complexity, low memory requirement and no training data requirement of the conventional MPPs is a value addition to their case.

**Table 6.6 Comparative Analysis of the Designed MPPT Techniques**

| Controller | MPP Tracking Efficiency | Computational Time | Settling Time | Complexity | Memory Requirement | Training Data Requirement |
|---|---|---|---|---|---|---|
| **P&O** | High | High | Very High | Least | Low | Nil |
| **InC** | High | Low | High | Least | Low | Nil |
| **49 rule FLC** | Higher | High | Low | High | High | Nil |
| **4 rule FLC** | High | Low | Low | Least | Least | Nil |
| **Proposed SOFLC** | Higher | Low | Least | Low | Low | Nil |
| **LM based ANN** | Higher | Least | Low | Low | Low | High |
| **BR based ANN** | Higher | Least | Low | Low | Low | High |
| **SCG based ANN** | Higher | Least | Low | Low | Low | High |
| **ANFIS** | Highest | Very High | Low | High | High | Very High |

FLCs and ANNs have a higher tracking efficiency. On one hand, the ANNs have a low computational time but on the other hand, their training data requirements are large. While FLCs, due to their inherent adaptivity and user-defined rules about the process require no training data. However, the 49 rule FLC which is modelled as a tradeoff between the complexity and accuracy of the control action has a high computational burden compared to the ANN. In the case of ANFIS based controllers, the highest tracking efficiency is offered at a low settling time owing to the hybrid combination of the two main AI based controllers i.e., FLCs and ANNs. But, the memory requirement and thus the computational burden is the highest. Additionally, the ANFIS based controller also require a training data set. Thus, a 4 rule FLC is developed and it is observed that though it offers a lesser tracking efficiency compared to the 49 rule FLC, it offers a less complex structure and thus a reduced computational burden and least computational time without the requirement of any training data. Thus, an attempt is made to develop a 4-rule FLC with a compensating polynomial. This controller with a cascaded compensating polynomial has been named as Simplified Optimized FLC (SOFLC) due to its simplified structure and optimized performance. SOFLC offers an approximate control action as a 49 rule FLC with a reduced complexity in the structure. It takes a low computational time and the least settling time. There is a low memory requirement for a SOFLC and no requirement of training data adds to their case.

# Chapter 7

# Conclusion & Future Scope of Work

## 7.1 CONCLUSION

AI based techniques have an edge over the conventionally established techniques like P&O and InC MPP techniques. This is due to their inherent capability of handling non-linearities in a better and effective manner. However, further improvement in the existing AI techniques can be incorporated in an attempt to optimize as well as simplify the complex structure of the AI based control models. In such an attempt, a simplified as well as optimized FLC with merely 4 rules has been proposed and developed. This not only approximates the response of a 49 rule FLC but also reduced the complex structure and henceforth, reduces the computational time and burden of the existing AI based MPP techniques.

It is also observed that with proper tuning of the incremental duty, even the conventional techniques like P&O and InC are able to track the MPP. However, there still lies a gap between the conventional and AI techniques due to the large tracking time taken by the conventional MPP techniques as compared to their counterparts.

## 7.2 FUTURE SCOPE OF WORK

The future scope of work may include but not be limited to:

- Extension of the proposed work to Type-II Fuzzy systems
- Use of the proposed technique to ANNs to have a faster and robust controller.
- Grid integration of the designed system using the proposed AI technique.
- Experimental verification of simulated techniques

# References


[1] S. Manish, I. R. Pillai, and R. Banerjee, "Sustainability analysis of renewables for climate change mitigation," *Energy for Sustainable Development*, vol. 10, no. 4, pp. 25–36, 2006.

[2] IEA, Global Energy & $CO_2$ Status Report 2019, IEA, Paris.

[3] Wayan G. Santika, M.Anisuzzaman, Parisa A.Bahri, G.M.Shafiullah, Gloria V.Rupf, Tania Urmee, "From goals to joules: A quantitative approach of interlinkages between energy and the Sustainable Development Goals," *Energy Research & Social Science*, vol. 50, pp. 201–214, 2019.

[4] Ministry of Power, Power Sector at a Glance ALL INDIA 2021, https://powermin.gov.in/en/content/power-sector-glance-all-india.

[5] M. Malinowski, J. I. Leon, and H. Abu-Rub, "Solar Photovoltaic and Thermal Energy Systems: Current Technology and Future Trends," *Proceedings of the IEEE*, vol. 105, no. 11, pp. 2132–2146, 2017.

[6] N. Jain, S. N. Singh, and S. C. Srivastava, "A generalized approach for DG planning and viability analysis under market scenario," *IEEE Trans.Ind. Electron.*, vol. 60, no. 11, pp. 5075–5085, Nov. 2013.

[7] G. G. Pozzebon, A. F. Q. Goncalves, G. G. Pena, N. E. M.Mocambique, and R. Q. Machado, "Operation of a three-phase power converter connected to a distribution system," *IEEE Trans. Ind. Electron.*, vol. 60, no. 5, pp. 1810–1818, May 2013.

[8] D. Espinoza, E. Barcenas, D. Campos-Delgado, and C. De Angelo, "Voltage-oriented input-output linearization controller as maximum power point tracking technique for photovoltaic systems," *IEEE Trans. Ind. Electron.*, vol. 62, no. 6, pp. 3499–3507, Jun. 2015.

[9] H. Bellia, R. Youcef, and M. Fatima, "A detailed modeling ofphotovoltaic module using MATLAB," *NRIAG Journal of Astronomyand Geophysics*, vol. 3, no. 1, pp. 53–61, 2014.

[10] B. W. Franca, L. F. da Silva, M. A. Aredes, and M. Aredes, "An improved iUPQC controller to provide additional grid-voltage regulation as a STATCOM," *IEEE Trans. Ind. Electron.*, vol. 62, no. 3, pp. 1345–1352, Mar. 2015.

[11] C. Yang and K. M. Smedley, "A cost-effective single-stage inverter with maximumpower point tracking," *IEEE Trans. Power Electron.*, vol. 19, no. 5, pp. 1289–1294, Sep.2004.

[12] D. Casadei, G. Grandi, and C. Rossi, "Single-phase single-stage photovoltaicgeneration system based on a ripple correlation control maximum power point tracking,"*IEEE Trans. Energy Convers.*, vol. 21, no. 2, pp. 562–568, Jun. 2006.

[13] W. Libo, Z. Zhengming, and L. Jianzheng, "A single-stage three-phase gridconnected photovoltaic system withmodified MPPT method and reactive powercompensation," *IEEE Trans. Energy Convers.*, vol. 22, no. 4, pp. 881–886, Dec. 2007.

[14] H.-J. Chiu *et al.*, "Amodule-integrated isolated solar microinverter," *IEEE Trans.Ind. Electron.*, vol. 60, no. 2,pp. 781–788, Feb. 2013.

[15] R. Ayop and C. W. Tan, "Design of boost converter based on maximum power point resistance for photovoltaic applications," *Solar Energy*, vol. 160, pp. 322–335, 2018.

[16] D. W. Hart, *Power Electronics*. New York, NY: McGraw-Hill Professional, 2010.

[17] S. Sengar, "Maximum Power Point Tracking Algorithms for Photovoltaic System: A Review," *International Review of Applied Engineering Research*, vol. 4, no. 2, pp. 147–154, 2014.

[18] S. Lyden and M. E. Haque, "Modelling, parameter estimation and assessment of partial shading conditions of photovoltaic modules," *Journal of Modern Power Systems and Clean Energy*, vol. 7, pp. 55–64, 2018.

[19] M. Hlaili and H. Mechergui, "Comparison of Different MPPT Algorithms with a Proposed One Using a Power Estimator for Grid Connected PV Systems," *International Journal of Photoenergy*, vol. 2016.
[20] H. Ibrahim and N. Anan, "Variations of PV module parameters with irradiance and temperature," *Energy Procedia*, vol. 134, pp. 276–285, 2017.
[21] K.H. Hussein, I. Muta, T. Hoshino, M. Osakada "Maximum photovoltaic power tracking: an algorithm for rapidly changing atmospheric conditions,"*IEEE Proc Gener Transm Distrib 1995*, vol. 142, pp. 59–64.
[22] C. Hua, J. Lin, C. Shen, "Implementation of a DSP-controlled photovoltaic system with peak power tracking," *IEEE Trans Ind Electron 1998*, vol 45:99–107.
[23] C. Hua, J. Lin, "An on-line MPPT algorithm for rapidly changing illuminations of solar arrays," Renew Energy 2003, vol. 28, pp. 1129–42.
[24] N. Femia,, G. Petrone, G. Spagnuolo G, Vitelli M., "Optimization of perturb and observe maximum power point tracking method",IEEE Trans Power Electron2005, vol. 20:,pp. 963–73.
[25] J. Ahmed, Z. Salam, "An improved perturb and observe (P&O) maximum PowerPoint tracking (MPPT) algorithm for higher efficiency." *Applied Energy 2015*, vol. 150, pp. 97–108.
[26] W. Xiao and W. Dunford, "A modified adaptive hill climbing MPPT method for photovoltaic power systems," in *IEEE 35th Annual Power Electronics Specialists Conference*, 2004, pp. 1957-1963.
[27] T. Shimizu, O. Hashimoto, and G. Kimura, "A novel high-performance utility-interactive photovoltaic inverter system," *IEEE Transactions on Power Electronics*, vol. 18, no. 2, pp. 704–711, 2003.
[28] A. Ahmed, L. Ran, and J. Bumby, "Perturbation parameters design for hill climbing MPPT techniques,", *IEEE International Symposium on Industrial Electronics*, 2012, pp. 1819–1824.
[29] A. Safari and S. Mekhilef, "Simulation and Hardware Implementation of Incremental Conductance MPPT With Direct Control Method Using Cuk Converter," *IEEE Transactions on Industrial Electronics*, vol. 58, no. 4, pp. 1154–1161, 2011.
[30] Q. Mei, M. Shan, L. Liu, and J. M. Guerrero, "A novel improved variable step-size incremental-resistance MPPT method for PV systems," *IEEE Transactions on Industrial Electronics*, vol. 58, no. 6, pp. 2427–2434, 2011.
[31] K. Kobayashi, I. Takano, and Y. Sawada, "A study of a two stage maximum power point tracking control of a photovoltaic system under partially shaded insolation conditions," *Solar Energy Materials & Solar Cells*, vol. 90, pp. 2975–2988, 2006.
[32] T. K. Soon and S. Mekhilef, "A Fast-Converging MPPT Technique for Photovoltaic System Under Fast-Varying Solar Irradiation and Load Resistance," *IEEE Transactions on Industrial Informatics*, vol. 11, no. 1, pp. 176–186.
[33] K. S. Tey and S. Mekhilef, "Modified incremental conductance MPPT algorithm to mitigate inaccurate responses under fast-changing solar irradiation level," *Solar Energy*, vol. 101, pp. 333–342, 2014.
[34] S. Chaudhary and A. Singh, "Analysis of AI Techniques for Maximum Power Point Tracking Under Partial Shading Conditions," in *IEEE 17th India Council International Conference (INDICON)*, 2020.
[35] J. Ma, X. Pan, K. L. Man, X. Li, H. Wen, and T. O. Ting, "Detection and Assessment of Partial Shading Scenarios on Photovoltaic Strings," *IEEE Transactions on Industry Applications*, vol. 54, no. 6, pp. 6279–6289, 2018.
[36] M. Seyedmahmoudian, S. Mekhilef, R. Rahmani, R. Yusof, and E. T. Renani, "Analytical Modeling of Partially Shaded Photovoltaic Systems," *Energies*, vol. 6, no. 1, pp. 128–144, 2013.
[37] B. Kia and W. Ditto, "Nonlinear Computing and Nonlinear Artificial Intelligence," in *Robotics and Well-Being*, 2019, pp. 44–53.
[38] R. Alik, A. Jusoh, and T. Sutikno, "A Review on Perturb and Observe Maximum Power Point Tracking in Photovoltaic System," *TELKOMNIKA*, vol. 19, no. 5, pp. 745–751, 2015.
[39] M. A. Elgendy, B. Zahawi, and D. J. Atkinson, "Assessment of the Incremental Conductance Maximum Power Point Tracking Algorithm," *IEEE Transactions on Sustainable Energy*, vol. 4, no. 1, pp. 108–117, 2012.

[40] S. Khadidja, M. Mountassar, and B. M'hamed, "Comparative study of incremental conductance and perturb & observe MPPT methods for photovoltaic system," in *International Conference on Green Energy Conversion Systems (GECS)*, 2017.
[41] M. Mokhlis, M. Ferfra, and M. Chraygane, "Nonlinear Control of a Photovoltaic Pumping System under Partial Shading," in *International Renewable and Sustainable Energy Conference (IRSEC)*, 2017, pp. 1–7.
[42] S. Guo, T. Walsh, A. Aberle and M. Peters, "Analysing partial shading of PV modules by circuit modelling", 38th IEEE Photovoltaic Specialists Conference, pp. 2957-2960, 2012.
[43] A. Sen, S. Pradhan, and A. Kumar, "A Novel Curve Scanning Based Maximum Power Point Tracking Algorithm Under Partial Shading Conditions," in *IEEE First International Conference on Smart Technologies for Power, Energy and Control (STPEC)*, 2020.
[44] J. C. Teo, H. G. T. Rodney, V. H. Mok, V. K. Ramachandaramurthy and C. K. Tan, "Impact of Partial Shading on the P-V Characteristics and the Maximum Power of a Photovoltaic String", Energies, vol. 11, no .7, pp. 1-22, 2018.
[45] Ying, H., Fuzzy Control and Modeling: Analytical Foundations andApplications, New York: IEEE Press, 2000.
[46] Zadeh, L. A., ―Fuzzy sets, Information and Control, vol.8, 1965, pp. 38-53.
[47] Yen, J. and Langari, R., Fuzzy Logic: Intelligence, Control, and Information, Prentice Hall, New Jersey,1998.
[48] Zadeh, L.A., ―Outline of A New Approach to the Analysis of Complex Systemsand Decision Processes,IEEE Transactions on Systems, Man and Cybernetics, vol. SMC-3, No. 1, 1973, pp. 28-44.
[49] Lee, H. X., Gatland, H. B., ―A New Methodology for Designing a Fuzzy Logic Controller, IEEE Transactions on System, Man, Cybernetics, vol. 25, no. 3, March 1995, pp. 505-512.
[50] S. Haykin, *Neural Networks - A comprehensive foundation*. New Jersey : Prentice Hall, 1999.
[51] H. Khayyam *et al.*, "A Novel Hybrid Machine Learning Algorithm for Limited and Big Data Modeling with Application in Industry 4.0," *IEEE Acc*, vol. 8, pp. 111381–111393, 2020.
[52] R. K. Kharab, S. L. Shimi, S. Chatterji and M. F. Ansari, "Modeling ofsolar PV module and maximum power point tracking using ANFIS",Renewable and Sustainable Energy Reviews, vol. 33, pp. 602-612, 2014.
[53] J. S. R. Jang, "ANFIS: Adaptive-network-based fuzzy inference system," IEEE Transactionson Systems, Man and Cybernetics, vol. 23, pp. 665-685, 1993.
[54] K. Benmouiza and A. Cheknane, "Clustered ANFIS network using fuzzy c-means, subtractive clustering, and grid partitioning for hourly solar radiation forecasting," *Theoretical and Applied Climatology*, vol. 137, pp. 31–43, 2019.
[55] C. Kavitha, T. S. Frank Gladson, and M. Prasanna Jeyanthi, "Analysis of Adaptive Neuro-Fuzzy Inference System for the Prediction of Hybrid Composites," *Advances in Mathematics: Scientific Journal*, vol. 9, no. 3, pp. 1857–8365, 2020.
[56] E. Sariev and G. Germano, "Bayesian regularized artificial neural networks for the estimation of the probability of default," *Quantitative Finance*, vol. 20, no. 2, pp. 311–328, 2019.
[57] Y. H. Kim, S. C. Ahn, and W.-H. Kwon, "Computational Complexity of General Fuzzy Logic Control and Its Simplification for a Loop Controller," *Fuzzy Sets and Systems*, vol. 111, no. 2, pp. 215–224, 2001.
[58] R. Singh, A. K. Singh and P. Kumar, "Self-tuned approximated simplest fuzzy logic controller based shunt active power filter," *International Conference on Energy Economics and Environment (ICEEE)*, pp. 1-6, 2015.

# Publications

## 1. Published Work

S. Chaudhary and A. Singh, "Analysis of AI Techniques for Maximum Power Point Tracking Under Partial Shading Conditions," in *IEEE 17th India Council International Conference (INDICON)*, 2020.

## 2. Accepted Work

S. Chaudhary and A. Singh, "Simplified Optimized Fuzzy Logic Controller for Maximum Power Point Tracking in PV Array under Partial Shading Conditions," in *IEEE Mysore Sub Section International Conference MysuruCon*, 2021.

## 3. Communicated

S. Chaudhary and A. Singh, "Design and performance analysis of artificial intelligence based maximum power point tracking algorithms for solar array under partial shading conditions ," in International Journal of Power and Energy Conversion, 2021.

## 4. Extended Consideration

S. Chaudhary and A. Singh, "Analysis of AI Techniques for Maximum Power Point Tracking Under Partial Shading Conditions," in *IEEE 17th India Council International Conference (INDICON)*, 2020 being considered for publication in IEEE Transactions on Industry Applications (TIA) or the IEEE Industry Applications Magazine.